Acta Pharmaceutica Sinica B 2025;15(9):4692−4710

Chinese Pharmaceutical Association
Institute of Materia Medica, Chinese Academy of Medical Sciences

Acta Pharmaceutica Sinica B

www.elsevier.com/locate/apsb
www.sciencedirect.com

ORIGINAL ARTICLE

Astrocytic dopamine D1 receptor modulates glutamatergic transmission and synaptic plasticity in the prefrontal cortex through D-serine

Yanan Yin[a,c,†], Jian Hu[a,†], Haipeng Wu[a], Xinyu Yang[a], Jingwen Qi[a], Lang Huang[a], Zhengyi Luo[a], Shiyang Jin[a], Nengyuan Hu[a], Zhoucai Luo[a], Tong Luo[a], Hao Chen[a], Xiaowen Li[a], Chunhua Yuan[a], Shuji Li[a], Jianming Yang[a], Yihua Chen[a,*], Tianming Gao[a,b,c,*]

[a]*State Key Laboratory of Multi-Organ Injury Prevention and Treatment, Key Laboratory of Mental Health of the Ministry of Education, Guangdong−Hong Kong−Macao Greater Bay Area Center for Brain Science and Brain-Inspired Intelligence, Guangdong−Hong Kong Joint Laboratory for Psychiatric Disorders, Guangdong Provincial Key Laboratory of Psychiatric Disorders, Guangdong Basic Research Center of Excellence for Integrated Traditional and Western Medicine for Qingzhi Diseases, Department of Neurobiology, School of Basic Medical Sciences, Southern Medical University, Guangzhou 510515, China*
[b]*Institute of Brain Diseases, Nanfang Hospital, Southern Medical University, Guangzhou 510515, China*
[c]*The Affiliated Brain Hospital, Guangzhou Medical University, Guangzhou 510370, China*

Received 7 February 2025; received in revised form 9 May 2025; accepted 27 May 2025

KEY WORDS

Astrocyte;
Dopamine D1 receptor;
mPFC;
Synaptic transmission;
Synaptic plasticity;
D-Serine;
Mental disorders

Abstract The prefrontal cortex (PFC) plays a pivotal role in orchestrating higher-order emotional and cognitive processes, a function that depends on the precise modulation of synaptic activity. Although pharmacological studies have demonstrated that dopamine signaling through dopamine D1 receptor (DRD1) in the PFC is essential for these functions, the cell-type-specific and molecular mechanisms underlying the neuromodulatory effects remain elusive. Using cell-type-specific knockout mice and patch-clamp recordings, we investigated the regulatory role of DRD1 on neurons and astrocytes in synaptic transmission and plasticity. Furthermore, we explored the mechanisms by which DRD1 on astrocytes regulate synaptic transmission and plasticity at the cellular level, as well as emotional and

*Corresponding authors.
E-mail addresses: tgao@smu.edu.cn (Tianming Gao), chenyihua@smu.edu.cn (Yihua Chen).
[†]These authors contributed equally to this work.

Peer review under the responsibility of Chinese Pharmaceutical Association and Institute of Materia Medica, Chinese Academy of Medical Sciences.

https://doi.org/10.1016/j.apsb.2025.07.034

cognitive functions at the behavioral level, through two-photon imaging, microdialysis, high-performance liquid chromatography, transcriptome sequencing, and behavioral testing. We found that conditional knockout of the *Drd1* in astrocytes (CKO^{AST}) increased glutamatergic synaptic transmission and long-term potentiation (LTP) in the medial prefrontal cortex (mPFC), whereas *Drd1* deletion in pyramidal neurons did not affect synaptic transmission. The elevated level of D-serine in the mPFC of CKO^{AST} mice increased glutamatergic transmission and LTP through NMDA receptors. In addition, CKO^{AST} mice exhibited abnormal emotional and cognitive function. Notably, these behavioral changes in CKO^{AST} mice could be reversed through the administration of D-serine degrease to the mPFC. These results highlight the critical role of the astrocytic DRD1 in modulating mPFC synaptic transmission and plasticity, as well as higher brain functions through D-serine, and may shed light on the treatment of mental disorders.

1. Introduction

The prefrontal cortex (PFC) is part of the neocortex. It has undergone significant expansion relative to other regions of the cerebral cortex throughout evolution, reaching its greatest extent in the human brain[1-4]. The medial prefrontal cortex (mPFC), in particular, is thought to underlie complex higher brain functions[5], including cognition (*i.e.*, memory[6], executive functions[7], decision making[8], attention[9], flexibility[10], and goal-directed behavior[11,12]), emotion regulation[13,14], motivation[15], and reward[16]. Alterations in synaptic transmission and synaptic plasticity within the mPFC are associated with emotional abnormalities and impaired cognitive function[17-22]. Thus, precise regulation of synaptic transmission and plasticity is required.

The mPFC has high catecholamine levels and synthesis rates[23] and is sensitive to catecholamines, such as dopamine[20,24,25]. Dopamine plays a critical role in the regulation of higher brain function[26-29]. The perturbation of dopamine in the PFC mirrors the cognitive deficits induced by PFC lesions in primates[23]. Dopamine neurons projecting to the mPFC originate from the ventral tegmental area[30] and regulate synaptic transmission and plasticity *via* the release of dopamine[19,24]. The DRD1 is the most abundant dopamine receptor subtype expressed in the mPFC[31,32]. In previous studies on the modulation of synaptic transmission in the PFC by the DRD1, pharmacological methods have predominantly been employed[24,33,34]. However, such pharmacological interventions are characterized by limited specificity for the targeted receptors. Consequently, in these studies, the roles of different receptor subtypes could not be isolated, and dopamine receptor subtypes within specific cell populations could not be manipulated. The differences in synaptic transmission regulation by DRD1 on different types of cells within the mPFC remain unexplored. Moreover, the underlying regulatory mechanisms are not yet understood.

Nearly 90% of neurons in the mPFC are excitatory pyramidal neurons[35,36], and the number of pyramidal neurons expressing *Drd1* is significantly greater than that of interneurons[37]. In addition to neurons, glial cells are receiving increasing attention. Astrocytes are the most abundant type of glial cells in the central nervous system and are one component of tripartite synapses[38-40]. Transmitter receptors expressed on astrocytes can sense extracellular signals, which in turn are involved in regulating synaptic transmission and plasticity[41-43]. Astrocytes in the mPFC express DRD1[44]; however, the functions of these receptors in astrocytes remain to be explored.

Using mice which Cre recombinase is specifically expressed in pyramidal neurons or astrocytes[45], a conditional knockout (CKO) mouse construction strategy, electrophysiological recording, *in vivo* neurotransmitter detection, and behavioral tests, we found that the mPFC DRD1 in astrocytes rather than in pyramidal neurons were involved in regulating excitatory synaptic transmission, synaptic plasticity, emotion, and cognitive function, all of which were mediated by D-serine. Our findings demonstrate for the first time that the mPFC astrocytic DRD1 plays an essential role in the regulation of glutamatergic transmission and synaptic plasticity, as well as higher brain functions *via* D-serine.

2. Materials and methods

2.1. Mice

The experimental mice were provided with unrestricted access to food and water and were housed under standard laboratory conditions: 24 ± 1 °C, 12-h light-dark cycle. All experiments were conducted in strict accordance with the Regulations for the Administration of Experimental Animals (China) and were approved by the Animal Ethics Committee of Southern Medical University (Approval No. D2022130). Astrocyte conditional knockout *Drd1* mice (CKO^{AST}) were generated by crossing $Drd1^{flox/flox}$ and *Aldh1l1-CreERT2* mice. Pyramidal neurons conditional knockout *Drd1* mice (CKO^{PYR}) were generated by crossing $Drd1^{flox/flox}$ and $Camk2\text{-}CreERT^2$ mice. The genotype of the offspring was determined by performing PCR on DNA extracted from mouse tails, and the primers are provided in the Supporting Information (Supporting Information Table S1). To induce Cre expression in $Aldh1l1\text{-}CreERT2;Drd1^{flox/flox}$ and $Camk2\text{-}CreERT^2;Drd1^{flox/flox}$ mice, tamoxifen (Sigma-Aldrich, Darmstadt, Germany, T5648, 75 mg/kg) was administered to mice by intraperitoneal injection at postnatal Week 8.

2.2. Stereotaxic injection

Anesthetized mice were fixed in a stereotaxic apparatus (RWD, Shenzhen, China) to expose the skull, and small holes were drilled. For experiments involving drug injections into the mPFC, the guide cannula was placed at the mPFC (AP: 1.85 mm, ML: ±0.3 mm, DV: −2.5 mm) and fixed with dental cement. Mice received bilateral injections of 0.5 μL of drug at a rate of 0.1 μL/min. To ensure complete drug diffusion, the infusion

cannula was left in place for an additional 5 min after the microinfusion pump stopped. For the adeno-associated virus injections, a 5-μL Hamilton syringe (65460-02, Hamilton, USA) connected to a microinjector pump (KDS, Stoelting, USA) was used to bilaterally deliver viral vectors into the mPFC at a rate of 0.05 μL/min. Following injection, the needle was elevated by 0.1 mm and left in place for 10 min to facilitate viral diffusion before being slowly withdrawn. Mice were then allowed to recover for three weeks to ensure sufficient gene expression. The following viral vectors were used in this study: rAAV-Camk2-EGFP-WPRE-hGH polyA (PT-0290-250314, BrainVTA Co., China); rAAV- Camk2-EGFP-P2A-CRE-WPRE-hGH polyA (PT-0137-250314, BrainVTA Co., China); AAV2/5-GfaABC1D-EGFP (BC-0377, BrainCase Biotechnology Co., China); and AAV5-GfaABC1D-Cyto-GCaMP6f (BC-0378, BrainCase Biotechnology Co., China). AAV2/5-GfaABC1D-cre-EGFP and rAAV-hSyn-DIO-EGFP-WPRE-hGH polyA were generated by Shanghai SunBio Biomedical Technology Co. (Shanghai, China).

2.3. *Immunofluorescence*

After anesthesia, mice were perfused with PBS followed by 4% PFA. Brains were extracted, post-fixed, rinsed, and dehydrated in 30% sucrose solution. Coronal sections containing the mPFC (thickness: 40 μm) were prepared using a Leica CM1850 cryostat. The sections were washed and blocked for 2 h in a solution containing 10% normal goat serum and 0.3% Triton X-100, followed by overnight incubation with the primary antibody at 4 °C. After washing, the sections were incubated with the secondary antibody for 2 h. Samples were mounted in Vectashield mounting medium containing DAPI and observed using a laser confocal microscope (Nikon C2, Japan).

2.4. *Slice preparation*

Brain slices were prepared following previously established methods[46]. Promptly extract the brain and cool it in chilled modified artificial cerebrospinal fluid (ACSF) after anesthetizing the mice with pentobarbital at a dosage of 75 mg/kg *via* intraperitoneal injection. Using a VT-1000S vibratome (Leica), section the mPFC into coronal slices of 300 μm thickness in ice-cold modified ACSF containing (in mmol/L): 220 sucrose, 2 KCl, 12 $MgSO_4$, 0.2 $CaCl_2$, 1.3 NaH_2PO_4, 26 $NaHCO_3$, and 10 D-glucose. After washing, the slices were placed on nylon mesh and stored in a chamber with regular ACSF (in mmol/L: 126 NaCl, 3 KCl, 1 $MgSO_4$, 2 $CaCl_2$, 1.25 NaH_2PO_4, 26 $NaHCO_3$, and 10 D-glucose) at 34 °C for 30 min. Subsequently, the brain slices were further incubated for additional 60 min before recording at 25 ± 1 °C. All solutions were saturated with a 95% O_2/5% CO_2 (*v*/*v*) gas mixture. Unless otherwise specified, all chemicals used were purchased from Sigma−Aldrich.

2.5. *Ca^{2+} imaging in brain slices*

Transfer the brain slices to the recording chamber and perfuse with oxygenated ACSF. Astrocytes expressing GCaMP6f were selected for imaging. Two-photon calcium imaging was performed using an Olympus FV1200MPE microscope (Olympus, Japan) equipped with a 25 × water-immersion objective (1.05 NA). GCaMP6f was excited at 920 nm using a Mai Tai Ti: Sapphire laser. Images were acquired at a resolution of 512 pixels × 512 pixels with a temporal resolution of 0.625 s per frame. A glass pipette containing either ACSF or ACSF with SKF81297 (10 μmol/L) was positioned near a target astrocyte under white light guidance. DRD1 antagonists, SCH23390 (10 μmol/L), were applied in the bath. A pressure pulse (0.08 MPa, 2 s duration) was applied to locally deliver the solution. Fluorescence was recorded from 30 s before to 60 s after drug application. Time-lapse images were analyzed using Fiji software. Regions of interest (ROIs) were manually selected, and changes in fluorescence intensity were quantified as $\Delta F/F$, calculated using Eq. (1):

$$\Delta F / F = 100 \times (F_t - F_0) \ / \ F_0 \tag{1}$$

where F_t represents the fluorescence intensity at time point t, and F_0 is the average baseline fluorescence intensity before drug application.

2.6. *Electrophysiological recording*

Following brain slice preparation, the slices were transferred to the recording chamber and continuously perfused with oxygenated ACSF. Image the slices using an infrared differential interference contrast microscope (BX51WI; Olympus, Tokyo, Japan). Borosilicate glass pipettes with a resistance of 4−6 MΩ using a micropipette puller (P-97, Sutter Instruments, Novato, CA, USA). Also, utilize a MultiClamp 700B amplifier and a 1440A digital converter (Molecular Devices, San Jose, CA, USA) for the recordings.

For sEPSC recording, cells were held at −70 mV in the presence of 20 μmol/L BMI. The mEPSC recordings were made using the same pipette solution (in mmol/L: 130 K-gluconate, 20 KCl, 10 HEPES, 0.2 EGTA, 4 MgATP, 0.3 Na_3GTP, and 10 NaCreatine, pH 7.30, 285 mOsm) as the sEPSC recordings, with the addition of TTX to the recording solution. For sIPSC recording, cells were held at 0 mV in the presence of 50 μmol/L APV and 20 μmol/L CNQX, and the pipette solution contained (in mmol/L): 110 Cs_2SO_4, 0.5 $CaCl_2$, 2 $MgCl_2$, 5 EGTA, 5 HEPES, 5 TEA, and 5 ATP-Mg, pH 7.30, 285 mOsm.

For PPRs recording, EPSCs were induced in layer 5/6 cells by stimulation in layer 2/3 in the presence of 20 μmol/L BMI, and the pipette solution contained (in mmol/L): 115 $CsCH_3SO_3$, 20 CsCl, 10 HEPES, 2.5 $MgCl_2$, 10 sodium phosphocreatine, 5 QX-314, 4 Na_2ATP, 0.4 Na_3GTP, and 0.6 EGTA, pH 7.3, 285 mOsm. The ratio was calculated as [(*p*2/*p*1) × 100].

To detect evoked AMPAR currents, we held mPFC layer 5/6 pyramidal cells at −70 mV while stimulating in layer 2/3 with 20 μmol/L BMI. To detect evoked NMDAR-mediated EPSC, we held pyramidal cells at +40 mV with 20 μmol/L BMI and 10 μmol/L NBQX. The same pipette solution as that used for PPR recording. We measured the peak of the averaged AMPAR-mediated EPSC and NMDAR-mediated EPSC.

For NMDA puffs, the neurons were clamped at +40 mV. Use the same pipette solution as for PPR recordings. The drug delivery head, containing 50 μmol/L NMDA, was connected to the puff application system (ALA-VM8, Scientific Instrument, Schaumburg, IL, USA) and maintained at a fixed distance from the recorded cell. The application duration was 2 s.

For the induction of plasticity recordings, we employed a theta-burst stimulation (TBS) protocol in layer 2−3 of the mPFC, consisting of three trains delivered over a period of 2 min, each train comprising 13 bursts at 5 Hz, with each burst containing 4 pulses at 100 Hz. Before the delivery of TBS, electrical stimulation was administered every 30 s, and the current responses of

layer 5/6 pyramidal neurons were continuously recorded for 6−10 min to establish a baseline. Following the induction of TBS, the recording continued for an additional 30 min. Pyramidal cells were held at −70 mV with a pipette solution containing (in mmol/L): $CsCH_3SO_3$ 115, HEPES 10, ATP 4, CsCl 20, GTP 0.4, EGTA 10, pH 7.3, 285 mOsm.

2.7. Microdialysis

After anesthesia, mice were placed on a stereotaxic apparatus to expose the skull, and small holes were drilled. A guide cannula (CMA/7, CMA, Stockholm, Sweden) was implanted near the mPFC (AP: 1.85 mm, ML: ±0.3 mm, DV: 1.5 mm) and fitted with a dummy probe. Before dialysis, the dummy probe was removed, and a microdialysis probe (CMA/7, membrane length: 1 mm, CMA) was inserted through the guide cannula and connected to a CMA microinjection pump (CMA 402). ACSF was continuously infused through the microdialysis probe at a constant rate of 1 μL/min into the brain, and samples were automatically collected using a microfraction collector (CMA 142).

2.8. HPLC analysis

A chromatographic column (Agilent ZORBAX Eclipse AAA, 993400-902) is used. After derivatization with *o*-phthaldialdehyde (Sigma−Aldrich, P0657), the sample was eluted at a flow rate of 0.8 mL/min using a gradient elution program and analyzed using a fluorescence detector. Standard curves were made with standards of different concentrations of various amino acids, and the amino acid concentrations of the samples were determined by using these standards.

For the detection of monoamines, the HPLC system (Sykam, Eresing, Bavaria, Germany), glassy carbon working electrode (VT-03, 3 mm in diameter), electrode spacer (25 μm), pulse damper, *in situ* silver/silver chloride reference electrode, ADF filter (0.05 Hz), electrochemical detector (Antec Decade II SDC) were used. The mobile phase was eluted isocratically at 0.2 mL/min, and the measurement time was 15 min with an operating voltage of +0.56 V, and a volume of 20 μL was used for the direct up-loading and analysis of the samples.

D-Serine was separated and monitored using a reverse-phase HPLC based on a published article[47]. Samples were derivatized with *o*-phthaldialdehyde (Sigma−Aldrich, P0657) and Boc-Cys-OH (Sigma−Aldrich, 15411). A Thermo Fisher Accucore C18 column (17126-152130) was used. A linear gradient elution was performed from 100% Buffer A (6.5% acetonitrile, 0.1 mol/L sodium acetate buffer, 3% tetrahydrofuran, pH 6.2) to 60% buffer B (47% acetonitrile, 0.1 mol/L sodium acetate buffer, 3% tetrahydrofuran, pH 6.2) at a flow rate of 0.2 mL/min. Subsequently, the system was washed with 100% methanol and equilibrated for 10 min in 100% Buffer A. Fluorescence detection was carried out at an excitation wavelength of 443 nm and an emission wavelength of 344 nm.

2.9. Fluorescence-activated cell sorting

The papain (P4762, Sigma−Aldrich) digestion solution was prepared in advance and incubated at 37 °C for 30 min to activate the enzyme. Brain extraction was performed following the procedure for electrophysiological recordings, and the brain was placed in ice-cold, oxygenated ACSF containing APV, CNQX, and TTX. Coronal sections (300 μm) were cut using a Leica VT210. The PFC region was isolated using microdissecting forceps. Brain tissue was then digested in the papain solution and dissociated with a homemade pipette. Once dissociation was complete, culture medium with serum was added to halt the digestion. The cells were enriched by centrifugation (900 × *g*, 4 °C, 15 min) and then incubated with FcR blocking reagent and anti-ACSA-2-PE antibody on ice for 10 and 20 min, respectively. FACS sorting was performed using the Beckman MoFlo XDP cell sorter to isolate PE-positive cells. The sorted cells were further enriched by centrifugation (1000 × *g*, 4 °C, 5 min).

2.10. RNA sequencing

After sorting, astrocytes were lysed and RNA was extracted using the RNA extraction kit (Qiagen, Hilden, Germany, #74104). Libraries from different indices were multiplexed and loaded onto the Illumina HiSeq/Illumina NovaSeq/MGI2000 systems for sequencing with a 2 × 150 paired-end (PE) configuration. Transcript sequences in FASTA format were initially generated based on known GFF annotation files and then indexed. Using the indexed file as a reference, gene and isoform expression levels were quantified from the paired-end clean data with HTSeq (v0.6.1). Differential expression analysis was performed using the DESeq2 Bioconductor package, which models the data based on a negative binomial distribution. The analysis included data-driven prior distributions for dispersion and fold-change estimation. Genes with adjusted *P*-values (Padj) $\leq$ 0.05 were considered differentially expressed.

2.11. Behavioral assays

2.11.1. Open field test

The Versamax animal activity monitoring system (AccuScan Instruments) is a transparent glass box measuring 40 cm × 40 cm × 30 cm. At the start of the 5 min test, mice were gently placed in the central area of the box. The system automatically recorded the time spent in different areas of the box and the total distance traveled. Data were analyzed using VersaDat software.

2.11.2. Elevated plus maze test

The maze consisted of two crossed arms: enclosed arms with walls and open arms without walls, each measuring 5 cm × 30 cm in width and length. The maze was elevated 40 cm above the ground. Animal behavior tracking software (Ethovision XT, Noldus, USA) was used. According to previously established experimental methods[48], before the 5 min test, mice were gently placed face down in the central area, and their movement trajectories were tracked and analyzed using an infrared camera positioned above the maze.

2.11.3. Forced swimming test

Two transparent glass tanks (45 cm high, 19 cm in diameter) were used, each filled with water to a depth of 23 cm and maintained at a temperature of 23.5 ± 1 °C. Place an opaque partition between the two cylinders to prevent mice from interacting with each other during the experiment. Position a camera in an appropriate location directly in front of the two cylinders to ensure the clearest and highest resolution image can be captured. Before the 6 min test, gently lift the mouse by its tail and slowly place it into the cylinder. When the mouse touches the surface of the water, release the tail slowly. The immobility time accumulated by the mouse during the final 4 min will be used as the statistical indicator.

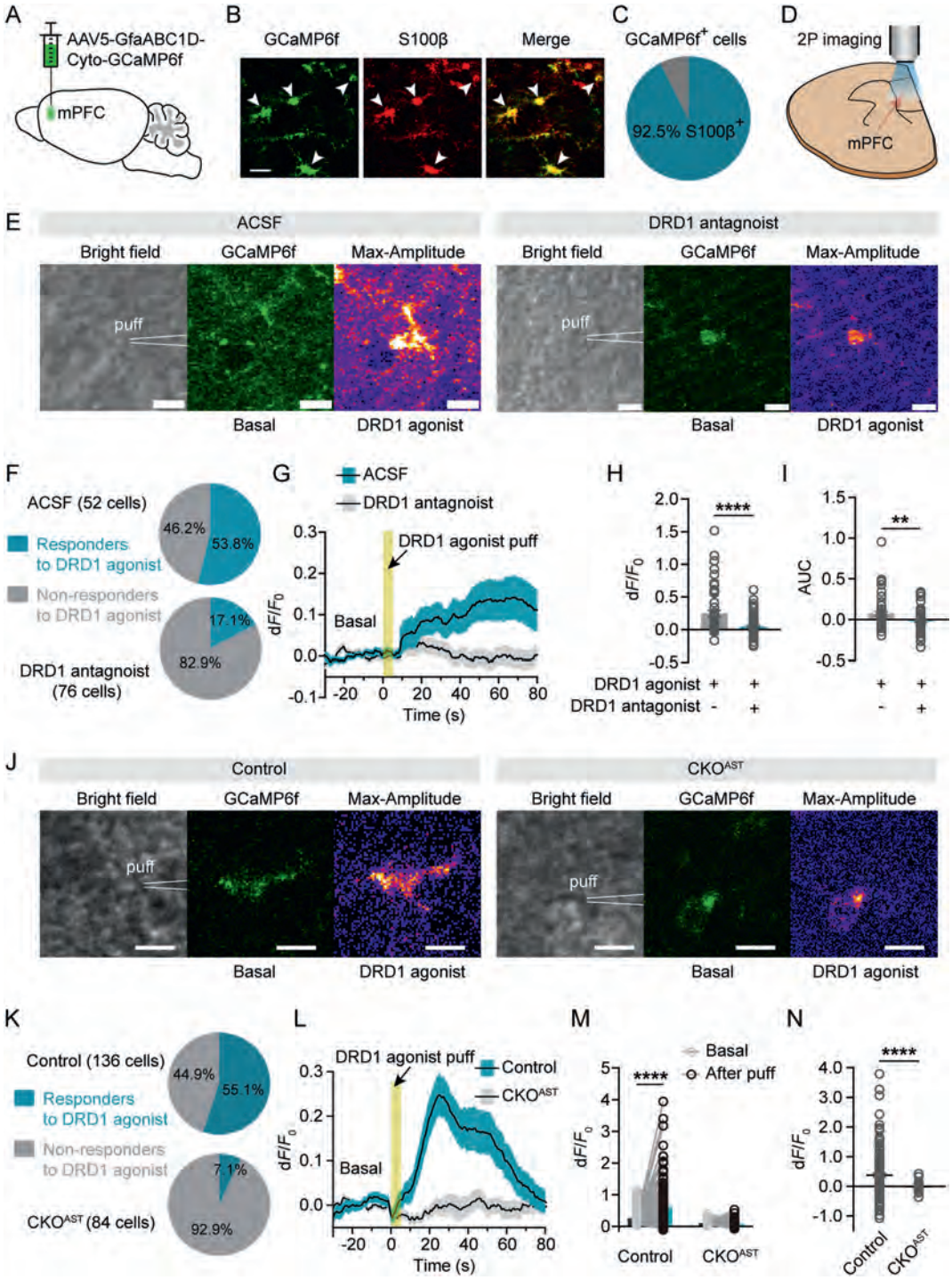

Figure 1 Astrocytic DRD1 regulates intracellular Ca^{2+} signal in the mPFC. (A) Schematic of the injection of an astrocyte-specific Ca^{2+} indicator virus into the mPFC. (B) Representative images showing the specificity of Ca^{2+} indicator expression in astrocytes. GCaMP6f, Ca^{2+} indicator; S100β, astrocyte marker. Scale bars, 20 μm. (C) Statistical analysis of co-localization between cells expressing the Ca^{2+} indicator and S100β-positive cells. (D) Schematic of *ex vivo* two-photon (2P) imaging of astrocytic Ca^{2+} signal in the mPFC. (E) Example images of Ca^{2+} signals in the mPFC astrocytes in response to puff-applied Dopamine D1 receptor (DRD1) agonists, both in the absence ("ACSF" refers to Artificial Cerebrospinal Fluid) and presence of DRD1 antagonists. The DRD1 agonist SKF81297 (10 μmol/L) and DRD1 antagonist SCH23390 (10 μmol/L) were used. Scale bar, 10 μm. (F) Proportion of activated astrocytes relative to the total cell count following exposure to DRD1 agonists in the absence or presence of DRD1 antagonists. (G–I) Quantification of the fluorescence amplitude and area under the curve of the Ca^{2+} signals. There were 52 cells without DRD1 antagonist incubation and 76 cells with DRD1 antagonist incubation. (G) Two-way ANOVA, F (1, 33908) = 974.6, $P < 0.0001$. (H) Mann–Whitney test, Mann–Whitney $U = 1057$, $P < 0.0001$. (I) Mann–Whitney test, Mann–Whitney $U = 1332$, $P = 0.006$. (J) Example images of Ca^{2+} signals in the mPFC astrocytes in response to puff-applied DRD1 agonists in control and CKO^{AST} mice. DRD1 agonist SKF81297 (10 μmol/L). Scale bar, 10 μm. (K) Proportion of activated astrocytes relative to the total cell count

2.11.4. Sucrose preference test

The testing was then divided into two stages: baseline measurement over the first four days, followed by a preference test for sugar water over the next three days. During the baseline stage, two bottles of purified water (W/W) were placed on the left and right sides of the cage on the first and second day, followed by two bottles of 1% sucrose solution (S/S) on the third and fourth day. The position of the bottles was exchanged daily to eliminate any position preference. On the fifth to seventh day, Bottle A was filled with water, while Bottle B was filled with 1% sucrose solution (S/W). The amount of liquid consumed was measured every 24 h, and the water and sucrose solutions were replaced. The preference ratio for sugar water was calculated as Eq. (2):

$$\text{The preference ratio for sugar water}\,(\%) = (\text{Volume of consumed sucrose solution VB} \,/\, (\text{Total volume of consumed water and sucrose solution VA} + \text{VB})) \times 100 \quad (2)$$

2.11.5. Y-maze test

The Y-maze consists of three identical arms (each measuring 38 cm × 7.6 cm) arranged at 120° angles. Spontaneous alternation behavior refers to the tendency of mice to sequentially explore different arms of the maze without repeating previous entries. Alternation is defined as consecutive entries into all three arms on overlapping triplet sets. Prior to the test, each mouse was individually placed at the center of the apparatus and allowed to freely explore the maze for 8 min. Arm entries were recorded manually.

2.12. RNA in situ hybridization

Following anesthesia, mice were perfused sequentially with ice-cold PBS and/or 4% paraformaldehyde (PFA). The brains were then removed and post-fixed in 4% PFA overnight at 4 °C. The next day, brains were dehydrated in 30% sucrose solution, followed by cryosectioning at a thickness of 10 μm. Sections were immersed in PFA fixative and incubated at 4 °C for 30 min. Dehydration was performed at room temperature using a graded ethanol series (50%, 70%, and 100%), each for 5 min. Pretreatment solution A was added to fully cover the sections and incubated at room temperature for 10 min. Sections were then treated with preheated 1 × Pretreatment solution B plus for 3 min. Next, 1 × Digestion Enzyme II was applied to the sections and incubated at 40 °C for 15 min. Probe hybridization was carried out at 40 °C for 2 h using the hybridization buffer. Reaction solution 1 was applied and incubated at 40 °C for 25 min, followed by Reaction solution 2 at 40 °C for 15 min. Type I Reaction solution 3 was then applied and incubated at 40 °C for 15 min. Fluorescence reaction buffer was added and incubated at room temperature in the dark for 30 min. If a Type II probe was used, the same steps were repeated as for the Type I probe. Sections were then blocked with 5% BSA and 0.1% Triton X-100 at 40 °C for 1 h, followed by incubation with primary antibodies (S100β, CaMK2, GFP) at 40 °C for 1 h. Secondary antibodies were also incubated at 40 °C for 1 h. Confocal imaging was performed, and statistical analysis was conducted. Cells with more than two intracellular fluorescent spots were defined as positive.

2.13. Western blot analysis

The lysed samples were boiled at 37 °C, centrifuged, and the supernatant was collected. Equal amounts of protein samples were separated by SDS-PAGE, followed by membrane transfer and blocking. The membranes were incubated overnight at 4 °C with a primary antibody (monoclonal anti-DRD1 antibody, 1:250, D2944, Sigma−Aldrich). Subsequently, an HRP-conjugated secondary antibody (1:2000; ab97057, Abcam) was incubated at room temperature in TBS for 1 h. A monoclonal anti-β-actin antibody (1:1000; A2228, Sigma−Aldrich) was applied on the same gel to normalize loading.

2.14. qRT-PCR and digital PCR

The reagents for RNA extraction, reverse transcription, and quantitative fluorescence detection were obtained from Takara. The instrument used was the 7500 system. β-Actin served as the endogenous control, and data were normalized using the ΔΔCt method. The required primers are provided in the supporting materials (Supporting Information Table S2). Digital PCR was carried out with EvaGreen Supermix (Bio-Rad, Hercules, CA, USA) on a QX200 system (Bio-Rad), and the data were analyzed using QUANTA software (Bio-Rad).

2.15. Protein analysis using wes (mini Western blot)

The sorted astrocytes were lysed in a buffer and crushed by repeated pipetting, followed by centrifugation at 16,000 × g for 30 min at 4 °C. Next, samples were loaded onto a 12-230 kDa Separation Module (ProteinSimple, San Jose, CA, USA) and detection using primary antibodies for mouse anti-DRD1 (1:50; D2944, Sigma−Aldrich) and mouse anti-actin (1:50; A2228, Sigma−Aldrich), along with the Anti-Mouse Detection Module (ProteinSimple). The relative abundance of DRD1 was calculated using Compass for SW software (version 4.0.0, ProteinSimple), with protein levels normalized to actin.

2.16. Statistical analysis

GraphPad Prism software was used. Firstly, the D'Agostino & Pearson omnibus normality test and F test were used to test the normality and homogeneity of variances of data samples from different groups, respectively. When the data met the criteria of normal distribution and homogeneity of variances, *t*-tests and one-way ANOVA were used. Two-way ANOVA was also used when appropriate. Data are presented as mean ± SEM. A *P*-value less than 0.05 was considered statistically significant. $*P < 0.05$, $**P < 0.01$, $***P < 0.001$, $****P < 0.0001$.

following exposure to DRD1 agonists in control and CKO^{AST} mice. (L−N) Quantification of the fluorescence amplitude of Ca^{2+} signals. There were 136 cells in control mice and 84 cells in CKO^{AST} mice. (L) Two-way ANOVA, F (1, 74627) = 1942, $P < 0.0001$. (M) control mice: Wilcoxon matched-pairs signed rank test, $W = 4796$, $P < 0.0001$. (N) Mann−Whitney test, Mann−Whitney $U = 3537$, $P < 0.0001$. Statistical details are in the supporting table. Data represent mean ± SEM, $**P < 0.01$, $****P < 0.0001$. mPFC, medial prefrontal cortex; DRD1, dopamine D1 receptor; CKO^{AST}, astrocyte-specific *Drd1* knockout mice.

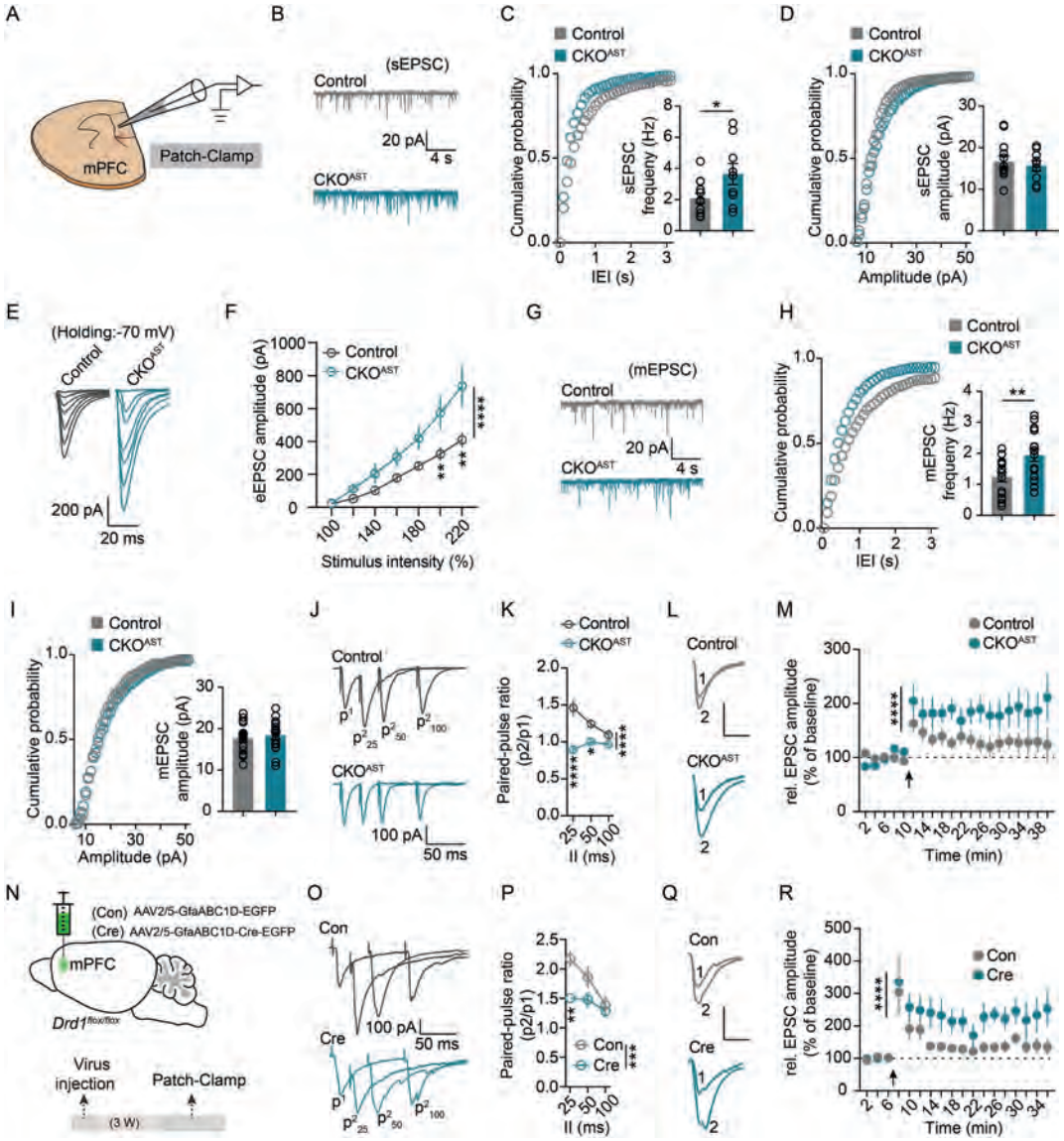

Figure 2 Astrocytic *Drd1*-deficient mice exhibit enhanced glutamatergic transmission and synaptic plasticity in the mPFC. (A) Schematic of whole-cell recordings. (B) Representative traces of spontaneous excitatory postsynaptic current (sEPSC) recorded from layer 5/6 pyramidal neurons in the mPFC of control and CKO^{AST} mice. (C, D) Cumulative probability distributions of the frequency (C) and amplitude (D) of sEPSC in mPFC layer 5/6 pyramidal neurons. $n = 12$ neurons from 4 control mice and $n = 9$ neurons from 3 CKO^{AST} mice, (C) Unpaired t test, $t = 2.225$, d$f = 19$, $P = 0.0384$. "IEI" stands for "Inter-event interval". (E) Representative traces of evoked EPSCs recorded from layer 5/6 pyramidal neurons in the mPFC of control and CKO^{AST} mice in response to increasing stimulus intensities, clamped at −70mV. (F) Input−output graphs showing increased evoked EPSC amplitude in CKO^{AST} mice compared with control mice. $n = 13$ neurons from 4 control mice and $n = 12$ neurons from 4 CKO^{AST} mice; two-way ANOVA, F (1, 142) = 30.94, $P < 0.0001$, Bonferroni post hoc test, 200%: $P = 0.0079$, 220%: $P = 0.0015$. (G) Representative traces of miniature excitatory postsynaptic current (mEPSC) in mPFC layer 5/6 pyramidal neurons from control and CKO^{AST} mice. (H, I) Cumulative probability distributions of the frequency (H) and amplitude (I) of mEPSC in mPFC layer 5/6 pyramidal neurons. $n = 16$ neurons of 4 control mice and $n = 17$ neurons of 4 CKO^{AST} mice, (H) Unpaired t test, $t = 2.809$, d$f = 31$, $P = 0.0085$. (J) Representative superimposed sweeps with three different inter-stimulus intervals of pair-pulse stimulations from control and CKO^{AST} mice. P^1 refers to the first evoked current, and P^2 refers to the second evoked current. (K) Paired−pulse ratio plotted against inter-stimulus intervals. $n = 9$ neurons of 3 control mice and $n = 10$ neurons of 3 CKO^{AST} mice, Two-way ANOVA, F (1,51) = 37.5, $P < 0.0001$, Bonferroni *post hoc* test, 25 ms: $P < 0.0001$, 50 ms: $P = 0.024$. II: Interpulse interval. (L, M) Representative traces (L) and diagram (M) showing the change over time in the amplitude of EPSCs measured before and after TBS (theta-burst stimulation) protocol from control and CKO^{AST} mice. $n = 10$ neurons from 6 mice of both groups, Two-way ANOVA, F (1, 328) = 33.26, $P < 0.0001$. '1' represents the averaged EPSC traces during the baseline phase, while '2' represents the averaged EPSC traces after TBS. Scale bars represent 50 ms, 40 pA. (N) Schematic diagram of virus injection into the mPFC and experimental workflow. Con virus: AAV2/5-GfaABC1D-EGFP; Cre virus: AAV2/5-GfaABC1D-Cre-EGFP. (O) Representative superimposed sweeps with three different inter-stimulus intervals of pair-pulse stimulations from two groups of mice. (P) Paired-pulse ratio plotted against inter-stimulus intervals. $n = 12$ neurons of 4 Con mice and $n = 13$ neurons of 4 Cre mice, Two-way ANOVA, F (1,69) = 11.89, $P = 0.001$, Bonferroni *post hoc* test, 25 ms: $P = 0.0029$. II: Interpulse interval. (Q, R) Representative traces (Q) and diagram (R) showing the change over

3. Results

3.1. Conditional knockout of Drd1 in astrocytes, but not in pyramidal neurons, increased glutamatergic transmission and long-term potentiation (LTP) in the mPFC

To investigate whether the DRD1 on pyramidal neurons is involved in regulating synaptic transmission, we first generated tamoxifen-inducible pyramidal neuron *Drd1*-deficient mice by crossing *Camk2-CreERT*^{2} mice with *Drd1*$^{flox/flox}$ mice. The specificity of *Camk2-CreERT*^{2} mice has been previously established[49]. We injected rAAV-hSyn-DIO-EGFP-WPRE-hGH polyA into the mPFC of *Camk2-CreERT*^{2} mice, resulting in Cre-expressing cells carrying EGFP. Co-labeling with *Slc17a7* (a marker for pyramidal neurons) revealed that 97.33% of EGFP-positive cells were pyramidal neurons, suggesting high specificity in *Camk2-CreERT*^{2} mice (Supporting Information Fig. S1). After several generations of breeding *Camk2-CreERT*^{2} mice and *Drd1*$^{flox/flox}$ mice, CKO^{PYR} (*Camk2-CreERT*^{2};*Drd1*$^{flox/flox}$) mice are obtained, with *Drd1*$^{flox/flox}$ mice as controls (Supporting Information Fig. S2A and S2B). Three weeks after tamoxifen treatment, Western blot analysis revealed that DRD1 levels were lower in the mPFC of CKO^{PYR} mice than in those of control mice (Supporting Information Figs. S2C−S2E, and S3). We then performed patch clamp, in a whole-cell configuration, to record spontaneous excitatory or inhibitory postsynaptic current (sEPSC or sIPSC, respectively) in the layer 5/6 pyramidal neurons in mPFC slices. Analysis of electrophysiological recordings revealed that there was no difference in the frequency or amplitude of sEPSC or sIPSC between the groups (Supporting Information Fig. S4). These results indicate that a deficiency of *Drd1* in pyramidal neurons may not affect the spontaneous synaptic transmission of pyramidal neurons in the mPFC.

To further confirm the role of DRD1 in pyramidal neurons in the mPFC in synaptic transmission. We used rAAV-CaMKIIa-EGFP-P2A-Cre[50,51] to selectively knock out *Drd1* in pyramidal neurons of the mPFC in *Drd1*$^{flox/flox}$ mice. Both the cell-type specificity of the Cre expression and the effective knockout of *Drd1* in pyramidal neurons but not in astrocytes within the mPFC were validated (Supporting Information Figs. S5 and S6). Electrophysiological results showed no changes in the frequency or amplitude of sEPSC or sIPSC (Supporting Information Fig. S7), which is consistent with our findings in the mPFC of CKO^{PYR} mice.

Astrocytes are the most abundant type of glial cell, and astrocytes in the PFC express *Drd1*[44] (Supporting Information Fig. S8). To further functionally validate the expression of DRD1 in astrocytes, we used AAV5-GfaABC1D-Cyto-GCaMP6f[52] viruses to express a Ca^{2+} indicator and detected the effects of DRD1 activation on Ca^{2+} signal in mPFC astrocytes (Fig. 1A). Immunofluorescence experiments revealed that 92.5% of the GCaMP6f-positive cells colocalized with the astrocytic marker S100β (Fig. 1B and C), confirming the specific expression of the Ca^{2+} indicator GCaMP6f in astrocytes. We inhibited action potentials with tetrodotoxin (TTX) to exclude potential involvement from neighboring neurons. Puffing the DRD1 agonist SKF81297 (10 μmol/L) onto mPFC slices induced an astrocytic Ca^{2+} signal, and this signal was blocked by the DRD1 antagonist SCH23390 (10 μmol/L) (Fig. 1D−I, Supporting Information Fig. S9A−S9C). These results suggest that DRD1 in astrocytes may play a role in regulating astrocytic Ca^{2+} signaling.

To further confirm the regulation of Ca^{2+} signaling by the astrocytic DRD1, we generated tamoxifen-inducible astrocytic *Drd1*-deficient mice by crossing *Aldh1l1-CreERT*^{2} mice with *Drd1*$^{flox/flox}$ mice (Supporting Information Fig. S10A−S10C). The specific expression of Cre recombinase in astrocytes was verified[45] (Supporting Information Fig. S11). Compared with those in control mice, the DRD1 levels in flow-sorted astrocytes from the PFC of CKO^{AST} mice were lower according to qPCR and mini-Western blotting (Fig. S10D−SG). To further confirm the knockout specificity, we performed RNAscope, and the results revealed that the expression of *Drd1* was reduced in astrocytes but not in neurons of the mPFC in CKO^{AST} mice (Supporting Information Fig. S12).

Puffing the DRD1 agonist SKF81297 (10 μmol/L) onto mPFC slices from control mice, but not in those from CKO^{AST} mice, increased astrocyte Ca^{2+} levels (Fig. 1J−N, Fig. S9D−S9F). These findings indicate that DRD1 in astrocytes are involved in the regulation of astrocytic Ca^{2+} signaling.

To elucidate the role of the astrocytic DRD1 in modulating synaptic transmission within the mPFC, we conducted electrophysiological recordings in both control and CKO^{AST} mice. Interestingly, compared with control mice, CKO^{AST} mice presented an increase in sEPSC frequency, but not amplitude, in mPFC pyramidal neurons (Fig. 2A−D). In addition, there was no difference in the frequency or amplitude of sIPSC between the groups of mice (Supporting Information Fig. S13). We also recorded the input (stimulus intensity)−output (amplitude) curve (*I−O* curve) of EPSCs at a holding potential of −70 mV. We found that the slope of the *I−O* curve was steeper in CKO^{AST} mice than in control mice (Fig. 2E and F), further indicating increased excitatory synaptic transmission.

To determine whether changes in excitatory synaptic transmission occur presynaptically or postsynaptically, we first compared miniature excitatory postsynaptic current (mEPSC) in mPFC pyramidal neurons between control and CKO^{AST} mice, and found that the frequency of mEPSC was increased in CKO^{AST} mice (Fig. 2G and H), whereas the amplitude of mEPSC did not change (Fig. 2I). Next, we performed paired-pulse recordings of EPSC evoked in mPFC pyramidal neurons. The recorded neurons responded to two consecutive stimulations at different intervals (25, 50, and 100 ms). Consistently, the paired-pulse ratios in CKO^{AST} slices were decreased compared with those in control slices (Fig. 2J and K). These observations indicate that the deletion of astrocytic DRD1 leads to increased presynaptic glutamate release.

Extensive research has demonstrated that the dopamine system is involved in the regulation of synaptic plasticity[24,53-55]. However, the role of dopamine receptors on astrocytes, particularly astrocytic DRD1, in modulating synaptic plasticity remains unclear. To investigate this issue, we recorded theta-burst stimulation (TBS)-induced LTP in mPFC slices from both control and

time in the amplitude of EPSCs measured before and after the TBS protocol from Con and Cre mice. For both groups, recordings were performed on 7 neurons derived from 4 individual mice. Two-way ANOVA, $F(1, 193) = 32.47$, $P < 0.0001$. '1' represents the averaged EPSC traces during the baseline phase, while '2' represents the averaged EPSC traces after TBS. Scale bars represent 50 ms, 40 pA. Statistical details are in the supplementary table. Data represent mean ± SEM, $^*P < 0.05$, $^{**}P < 0.01$, $^{***}P < 0.001$, $^{****}P < 0.0001$. mPFC, medial prefrontal cortex; CKO^{AST}, astrocyte-specific *Drd1* knockout mice.

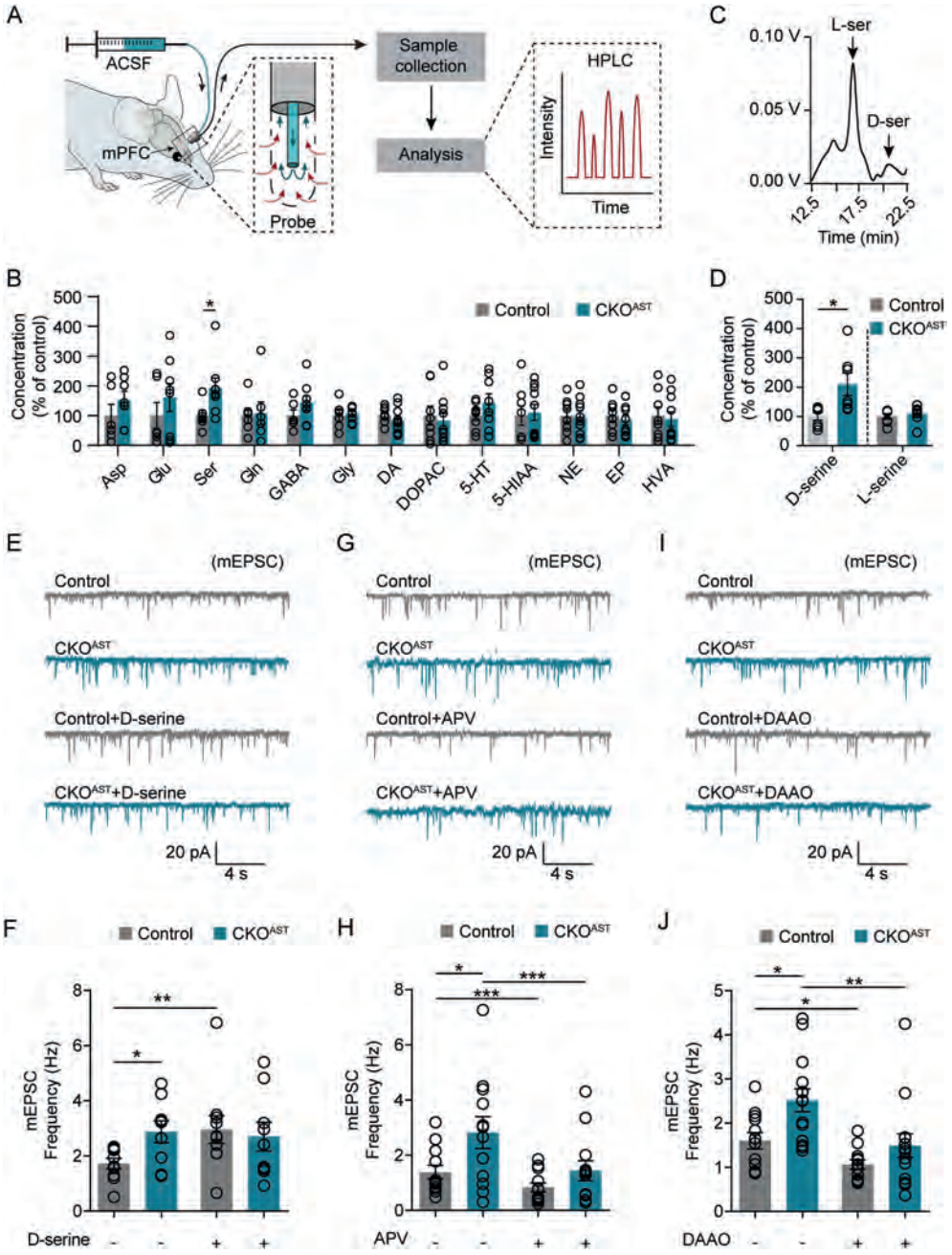

Figure 3 Astrocytic DRD1 modulates glutamatergic transmission through D-serine. (A) Schematic diagram of microdialysis and transmitters detection. (B) The amino acids and monoamine neurotransmitter levels in the mPFC from control and CKO^{AST} mice. Asp (aspartate), Glu (glutamate), Ser (serine), Gln (glutamine), GABA, Gly (glycine), DA (dopamine), DOPAC (3,4-dihydroxyphenylacetic acid), 5-HT (5-hydroxytryptamine), 5-HIAA (5-hydroxyindoleacetic acid), NE (norepinephrine), EP (epinephrine), HVA (homovanillicacid). $n = 6-10$ mice, Ser: Mann−Whitney test, Mann−Whitney $U = 6$, $P = 0.02$. (C) HPLC chromatogram showing L-serine and D-serine peaks. (D) HPLC detection showing D-serine and L-serine levels in the mPFC from two groups. 7 mice for each group. D-serine: Unpaired t test with Welch's correction, Welch-corrected, $t = 2.717$, d$f = 7.431$, $P = 0.0283$. (E) Representative traces of miniature excitatory postsynaptic current (mEPSC) from both groups before and after treatment with D-serine. (F) The effects of D-serine on the mEPSC frequency of mPFC layer 5/6 pyramidal neurons in control and CKO^{AST} mice. $n = 10$ neurons of 3 control mice and $n = 9$ neurons of 3 CKO^{AST} mice, control *versus* CKO^{AST} groups: Unpaired t test, $t = 2.705$, d$f = 17$, $P = 0.015$; control *versus* control + D-serine groups: Wilcoxon matched-pairs signed rank test, $W = 55$, $P = 0.002$. D-serine: 50 μmol/L. (G) Representative traces of mEPSC from both groups before and after treatment with the NMDAR antagonist APV. (H) The effects of APV (NMDAR antagonist, 100 μmol/L) on the mEPSC frequency of mPFC layer 5/6 pyramidal neurons in control and CKO^{AST} mice. $n = 12$ neurons of both groups from 4 pairs mice, control *versus* CKO^{AST} groups: Unpaired t test with Welch's correction, $t = 2.285$, d$f = 14.82$, $P = 0.0375$; control *versus* control + APV groups: Wilcoxon matched-pairs signed rank test, W $= -78$, $P = 0.0005$; CKO^{AST} *versus* CKO^{AST} + APV groups: Paired t test, $t = 5.013$, d$f = 11$, $P = 0.0004$. (I) Representative traces of mEPSC from both groups without or with the D-serine degrading enzyme, D-amino acid oxidase (DAAO). (J) The effects of DAAO (D-amino acid oxidase, 0.2 unit/mL) on the mEPSC

CKO^{AST} mice. Compared with that in the control group, LTP in CKO^{AST} mice was significantly greater (Fig. 2L and M), indicating that DRD1 on astrocytes are involved in the modulation of synaptic plasticity.

To further demonstrate the role of astrocytic DRD1 in the mPFC in synaptic transmission and plasticity at the cellular level, we used an adeno-associated virus (AAV-GfaABC1D-Cre[56,57]) to selectively knock out astrocytic *Drd1* in the mPFC of $Drd1^{flox/flox}$mice. Both the cell-type specificity of the Cre expression and the effective knockout of *Drd1* in astrocytes but not in neurons within the mPFC were validated (Supporting Information Figs. S14 and S15). We then conducted paired-pulse ratio experiments as well as synaptic plasticity assessments. In the Cre group, paired-pulse ratios were reduced (Fig. 2N−P), and LTP was increased (Fig. 2Q and R). These results indicate that astrocytic DRD1 in the mPFC contribute to the regulation of presynaptic glutamate release and synaptic plasticity.

3.2. Astrocytic DRD1 modulates presynaptic glutamate release and synaptic plasticity via D-serine

Gliotransmitters play a role in controlling synaptic transmission and plasticity[58-60]. To investigate how DRD1 in astrocytes regulates glutamatergic transmission, we utilized *in vivo* microdialysis to collect gliotransmitters that are known to be secreted by astrocytes in the mPFC of control and CKO^{AST} mice. The levels of amino acid neurotransmitters and monoamine neurotransmitters in the dialysate were subsequently analyzed using high-performance liquid chromatography (HPLC) (Fig. 3A). Compared with those in control mice, serine level was higher in CKO^{AST} mice, and no changes in other molecules were detected (Fig. 3B). Next, we further distinguished two configurations of serine, L-serine and D-serine (Fig. 3C). The D-serine level was higher in CKO^{AST} mice than in control mice, whereas the L-serine levels in the CKO^{AST} mice and control mice were similar (Fig. 3D). These results demonstrate that the astrocytic DRD1 modulates the extracellular D-serine level.

D-Serine is an endogenous coagonist of NMDA receptors (NMDARs)[60,61] and can promote the presynaptic release of glutamate by binding to presynaptic NMDARs (preNMDARs)[62,63]. To clarify whether the astrocytic DRD1 regulates presynaptic glutamate release through D-serine, we first compared the effects of D-serine treatment on mEPSC recorded in mPFC slices from both groups of mice. Adding D-serine increased the mEPSC frequency in mPFC slices from control mice to a level similar to that in slices from CKO^{AST} mice but did not affect the already elevated frequency of mEPSC in CKO^{AST} mice (Fig. 3E and F). Next, blocking the NMDAR with its antagonist APV decreased the mEPSC frequency in mPFC slices from both groups to a similar level (Fig. 3G and H). To further explore the impact of reducing D-serine levels on mEPSC frequency in mPFC slices from the two groups, we treated the slices with D-amino acid oxidase (DAAO)[60,64], which lowers D-serine levels. DAAO (0.2 unit/mL[60]) abolished the increased mEPSC frequency in CKO^{AST} slices and reduced the frequency in mPFC slices from both groups to a similar level (Fig. 3I and J). Notably, D-serine, APV, and DAAO did not affect the mEPSC amplitude (Supporting Information Fig. S16). These results indicate that the astrocytic DRD1 modulates presynaptic excitatory synaptic transmission through D-serine.

To determine whether astrocytic DRD1 regulates LTP through D-serine, we subsequently administered D-serine to the slices. This treatment elevated LTP in control mice to a degree comparable to that in CKO^{AST} mice but did not affect the already elevated LTP in CKO^{AST} mice (Fig. 4A and B). Next, we treated the slices with DAAO and found that this treatment blocked LTP induction in both the control and CKO^{AST} slices (Fig. 4C and D). These results demonstrate that the astrocytic DRD1 modulates synaptic plasticity *via* D-serine.

The increased synaptic plasticity in the mPFC of astrocytic *Drd1*-deficient mice (Figs. 2M and 4B) may be due to increased presynaptic glutamate release or heightened postsynaptic NMDAR activity resulting from elevated D-serine. There was no significant difference in EPSC amplitude between control and CKO^{AST} mice during the pre-TBS phase of LTP (Fig. 4E). This finding aligns with the previously recorded results of evoked EPSC currents at smaller stimulus intensities (Fig. 2F), suggesting that there was no obvious increase in presynaptic release in the astrocytic *Drd1*-deficient mice under the test stimulus. To test whether postsynaptic NMDAR activity was increased in astrocytic *Drd1*-deficient mice, we puffed NMDA (50 μmol/L) into mPFC brain slices from both groups of mice and recorded the induced currents at a holding potential of +40 mV, mimicking the depolarization induced by TBS for LTP induction. The data revealed that the current amplitudes recorded from CKO^{AST} mice were significantly greater than those recorded from control mice (Fig. 4F and G). Furthermore, we recorded the NMDAR currents at + 40 mV induced by an electrical stimulus and found that with increasing stimulus intensity, the CKO^{AST} mice exhibited greater NMDAR-EPSC (Fig. 4H and I). These results demonstrate that astrocytic DRD1 is involved in regulating postsynaptic NMDAR activity when postsynaptic neurons are depolarized.

Next, lowering D-serine levels with DAAO abolished the increase in NMDAR-EPSC in CKO^{AST} mice (Fig. 4J and K), suggesting that astrocytic DRD1 regulates postsynaptic NMDAR function by modulating D-serine levels, which may contribute to LTP induction.

3.3. RNA-sequencing of astrocytes provides potential molecular candidates for DRD1 regulation of D-serine levels

To investigate how DRD1 in astrocytes regulates D-serine levels, we performed transcriptome sequencing (RNA-Seq) on astrocytes isolated from the frontal cortex of control and CKO^{AST} mice by using fluorescence-activated cell sorting (FACS) (Fig. 5A−C). Serine racemase (SR) and DAAO are known to synthesize and degrade D-

frequency of mPFC layer 5/6 pyramidal neurons in control and CKO^{AST} mice. $n = 12$ neurons of 4 control mice and $n = 14$ neurons of 4 CKO^{AST} mice, control *versus* CKO^{AST} groups: Unpaired *t* test, $t = 2.785$, d$f = 24$, $P = 0.0103$; $n = 12$ neurons of 4 control + DAAO mice and $n = 14$ neurons of 4 CKO^{AST} + DAAO mice; control *versus* control + DAAO groups: Unpaired *t* test, $t = 2.533$, d$f = 22$, $P = 0.019$; CKO^{AST} *versus* CKO^{AST} + DAAO groups: Mann Whitney test, Mann−Whitney $U = 37$, $P = 0.0042$. Statistical details are in the supporting table. Data represent mean ± SEM, $*P < 0.05$, $**P < 0.01$, $***P < 0.001$. mPFC, medial prefrontal cortex; CKO^{AST}, astrocyte-specific *Drd1* knockout mice; HPLC, high-performance lipid chromatography; NMDAR, NMDA receptor.

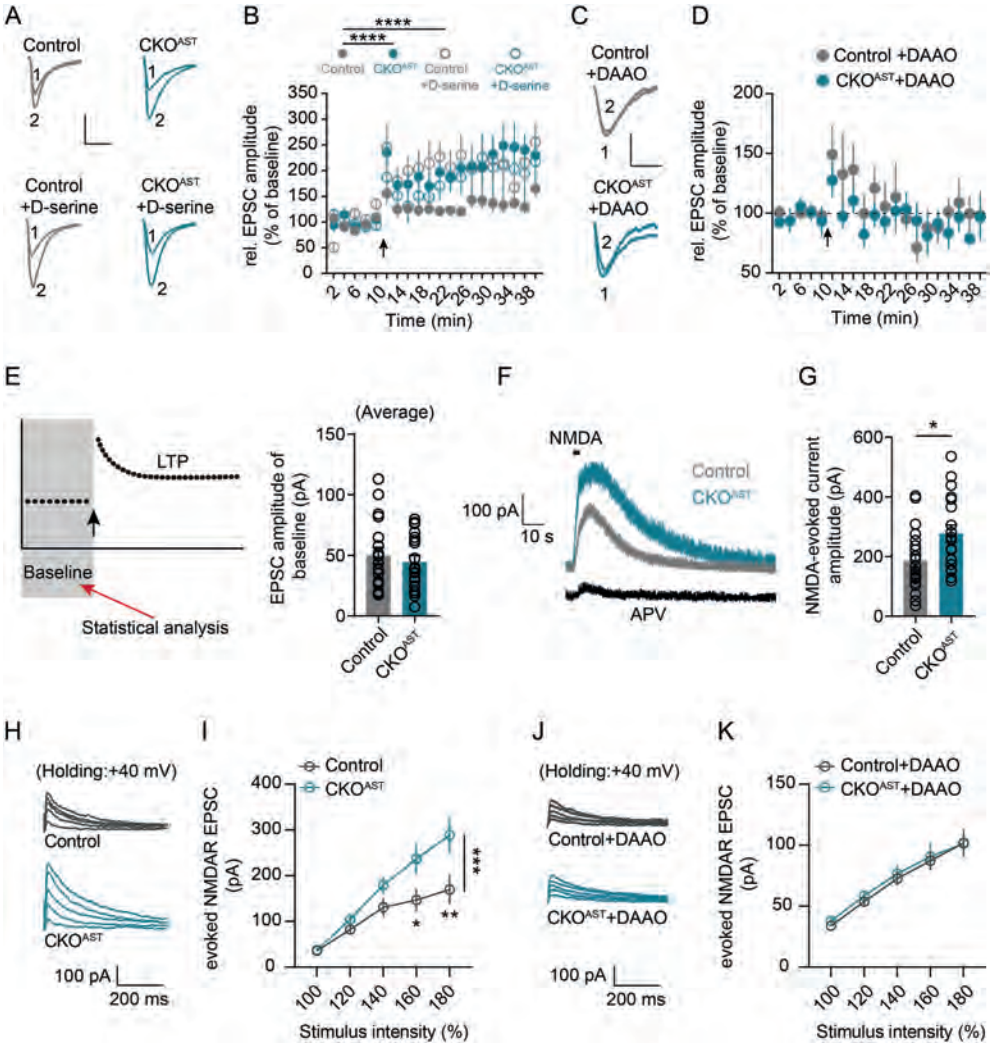

Figure 4 Astrocytic DRD1 modulates LTP and NMDA receptor activity through D-serine. (A, B) Representative traces (A) and diagram (B) showing the change over time in the amplitude of EPSCs measured before and after TBS protocol from control and CKO^{AST} mice, with or without D-serine (50 μmol/L) treatment. $n = 8$ neurons of 5 control mice and $n = 8$ neurons of 4 CKO^{AST} mice, control *versus* CKO^{AST} groups: Two-way ANOVA, F (1, 261) = 75.16, $P < 0.0001$; $n = 7$ neurons of 4 control + D-serine mice and $n = 6$ neurons of 4 CKO^{AST} + D-serine mice. control *versus* control + D-serine groups: Two-way ANOVA, F (1, 241) = 63.47, $P < 0.0001$. '1' represents the averaged EPSC traces during the baseline phase, while '2' represents the averaged EPSC traces after TBS. Scale bars represent 50 ms, 40 pA. (C, D) Representative traces (C) and a diagram (D) showing the effect of DAAO (D-amino acid oxidase, 0.2 unit/mL) on the amplitude of EPSCs measured before and after TBS from control and CKO^{AST} mice. $n = 9$ neurons from 4 mice of both genotypes. '1' represents the averaged EPSC traces during the baseline phase, while '2' represents the averaged EPSC traces after TBS. Scale bars represent 50 ms, 40 pA. (E) Statistical analysis of the average EPSC values during the 10-min baseline recording of LTP in control and CKO^{AST} mice. $n = 18$ neurons of 11 control mice and $n = 18$ neurons of 10 CKO^{AST} mice. (F) Example of currents evoked by a 2-s puff of NMDA at +40 mV, which are sensitive to APV. (NMDA: 50 μmol/L, APV: 100 μmol/L). (G) Statistical analysis of the NMDA-evoked currents in control and CKO^{AST} mice. $n = 20$ neurons of 4 control mice and $n = 19$ neurons of 4 CKO^{AST} mice; Unpaired t test, $t = 2.512$, d$f = 37$, $P = 0.0165$. (H) Representative traces of NMDAR-mediated EPSCs evoked with increasing stimulus intensities in mPFC layer 5/6 pyramidal neurons from control and CKO^{AST} mice, clamped at +40 mV. (I) Input−output graphs showing increased amplitude of stimulus-evoked NMDAR EPSCs from CKO^{AST} compared to control mice ($n = 10$ neurons of 4 control mice and $n = 12$ neurons of 4 CKO^{AST} mice; Two-way ANOVA, F (1, 98) = 14.25, $P = 0.0003$, Bonferroni post hoc test, 160%: $P = 0.0380$, 180%: $P = 0.0043$). (J) Representative traces of NMDAR-mediated EPSCs evoked with increasing stimulus intensities in mPFC layer 5/6 pyramidal neurons treated with DAAO (0.2 unit/mL) from control and CKO^{AST} mice, clamped at +40 mV. (K) Input−output graphs showing similar amplitude of stimulus-evoked NMDAR EPSCs from the two groups treated with DAAO ($n = 13$ neurons of 4 mice for both genotypes). Statistical details are in the supporting table. Data represent mean ± SEM, $^*P < 0.05$, $^{**}P < 0.01$, $^{***}P < 0.001$, $^{****}P < 0.0001$. CKO^{AST}, astrocyte-specific *Drd1* knockout mice; LTP, long-term potentiation; NMDAR, NMDA receptor; EPSCs, excitatory postsynaptic currents.

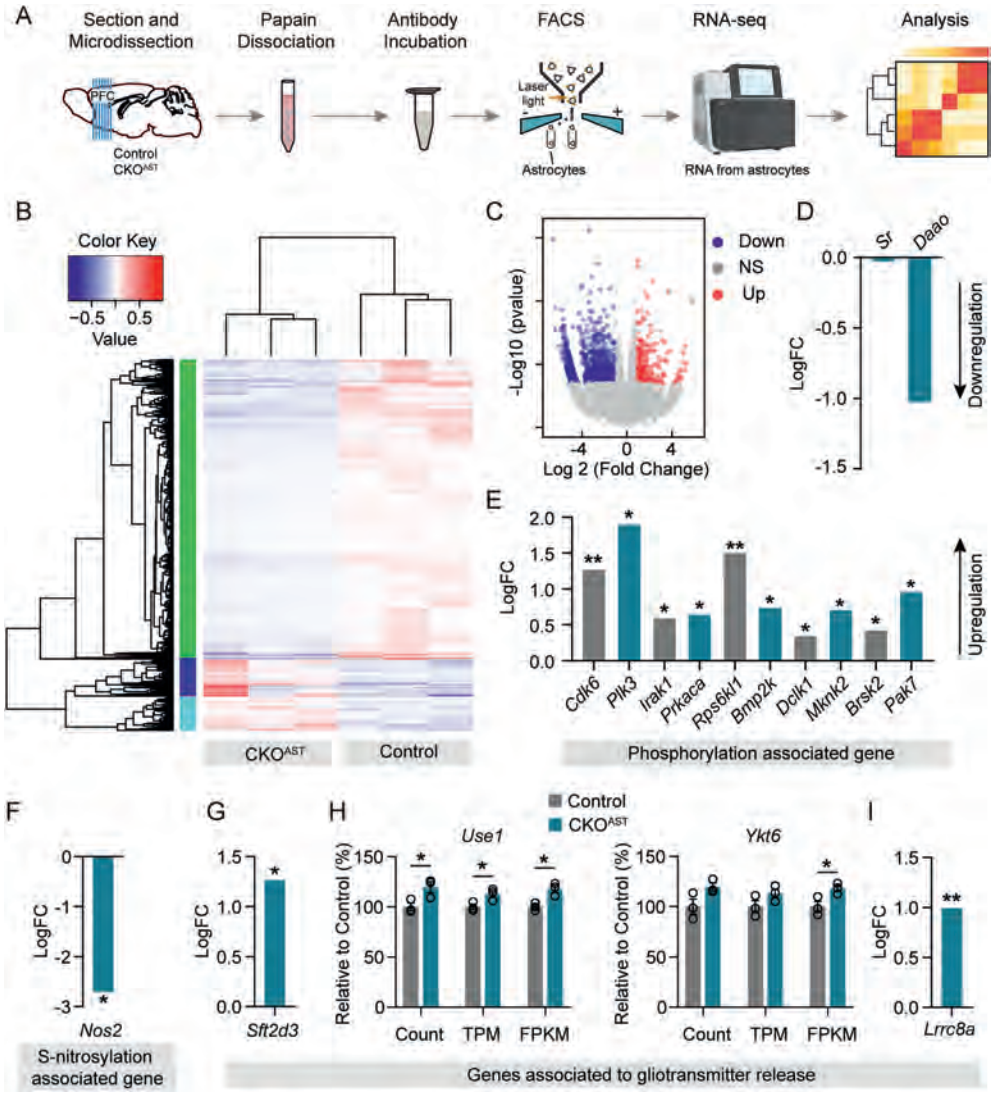

Figure 5 Altered genes potentially regulating serine racemase activity and gliotransmitter release in the astrocytes of CKO^{AST} mice. (A) The experimental procedure for transcriptome sequencing of astrocytes from control and CKO^{AST} mice. FACS stands for fluorescence-activated cell sorting. (B) Heatmap showing the transcriptome profiles of control and CKO^{AST} mice. (C) Volcano plots of differentially expressed genes (DEGs) between control and CKO^{AST} mice. Blue and red dots indicate significantly down- and up-regulated genes, respectively. (D) The expression levels of the *Sr* and *Daao* genes remained unchanged. (E) Upregulated threonine phosphorylation-associated genes among the DEGs. *Cdk6* (cyclin dependent kinase 6), *Plk3* (polo like kinase 3), *Irak1* (interleukin-1 receptor-associated kinase 1), *Prkaca* (protein kinase, cAMP dependent, catalytic, alpha), *Rps6kl1* (ribosomal protein S6 kinase-like 1), *Bmp2k* (BMP2 inducible kinase), *Dclk1* (doublecortin-like kinase 1), *Mknk2* (MAP kinase-interacting serine/threonine kinase 2), *Brsk2* (BR serine/threonine kinase 2), *Pak7* (p21 (RAC1) activated kinase 7). (F) The *Nos2* (nitric oxide synthase 2, inducible) gene is downregulated among the DEGs. (G–I). Upregulated genes associated with gliotransmitter release among the DEGs. (G). *Sft2d3* (SFT2 domain containing 3), (H) *Use1* (unconventional SNARE in the ER 1 homolog), *Ykt6* (YKT6 v-SNARE homolog), (I) *Lrrc8a* (leucine rich repeat containing 8A VRAC subunit A). Count (Raw Counts), TPM (Transcripts Per Million), FPKM (Fragments Per Kilobase of transcript per Million mapped reads). Statistical details are in the supporting table. *$P < 0.05$, **$P < 0.01$. CKO^{AST}, astrocyte-specific *Drd1* knockout mice.

serine, respectively[65]. RNA-Seq analysis revealed no changes in the expression levels of *Sr* or *Daao* after the deletion of *Drd1* in astrocytes (Fig. 5D), which is consistent with our findings in mPFC brain tissue (Supporting Information Fig. S17). These findings suggest that *Drd1* in astrocytes may not directly influence the expression of genes involved in D-serine synthesis or degradation.

Furthermore, most known regulations of D-serine levels focus on the modulation of SR activity[65,66]. The phosphorylation of SR at threonine sites can stimulate the production of D-serine[67]. RNA-Seq analysis revealed an increase in the expression levels of kinases capable of phosphorylating threonine residues (Fig. 5E). Another mechanism for regulating SR activity is *S*-nitrosylation. nitric oxide (NO) is an unconventional signaling molecule that reacts with cysteine residues through a process known as *S*-nitrosylation[68]. SR has been identified as an *in vivo* target of NO, which inhibits SR activity through nitrosylation[69]. This

nitrosylation is believed to be dependent on nitric oxide synthase (NOS)[70]. Additionally, RNA-Seq analysis revealed that the *Nos2* gene expression was reduced in CKO^{AST} mice (Fig. 5F), suggesting that *S*-nitrosylation may be decreased, thereby leading to a disinhibition of SR activity.

In addition, we analyzed genes associated with gliotransmitter release and found that the expression levels of the vesicle release-related gene *Sft2d3* were elevated in CKO^{AST} mice (Fig. 5G). The expression of genes associated with SNARE, *Use1*, and *Ykt6* was also upregulated (Fig. 5H). In addition, D-serine can be released through alternative non-exocytotic pathways, such as volume-regulated anion channels (VRACs)[71]. The expression of the *Lrrc8a* gene, one of the subtypes of VRAC, was significantly upregulated (Fig. 5I). Previous research has indicated that the activation of VRAC promotes nonvesicular D-serine release[72].

These results suggest that astrocytic DRD1 may regulate D-serine levels either by mediating the modulation of SR activity or by regulating the release of D-serine through vesicular or nonvesicular pathways.

3.4. Astrocytic DRD1 in the mPFC modulates anxiolytic-like behaviors, passive coping responses, and cognitive function via D-serine

The mPFC is closely associated with emotion and cognition (*i.e.*, memory) regulation[19,57,73-75]. To further investigate the *in vivo* function of the astrocytic DRD1, we first tested the anxiety-like behavior of CKO^{AST} in the open field test (OFT) and the elevated plus maze (EPM) test. Compared with control mice, CKO^{AST} mice displayed an unchanged total distance traveled (Fig. 6A and B), but an increased travel duration in the center zone of the box (Fig. 6C), indicating that the astrocytic DRD1 modulates anxiety-like behavior in these mice. Moreover, CKO^{AST} mice spent increased amounts of time in the open arms (Fig. 6D and E) and made more crosses of the open arms (Fig. 6F) in the EPM test, further confirming the anxiolytic-like phenotype of CKO^{AST} mice.

Compared with control mice, CKO^{AST} mice displayed a significantly decreased immobile time in the forced swimming test (FST) compared to control mice (Fig. 6G and H) but no change in consumption of sucrose water in the sucrose preference test (Supporting Information Fig. S18). Next, we also observed working memory impairment in CKO^{AST} mice, as evidenced by a decrease in spontaneous alternation performance in the Y-maze test (Fig. 6I and J). In summary, CKO^{AST} mice displayed anxiolytic-like behavior, reduced passive coping response, and impaired cognitive functions.

To determine the necessity of the mPFC in the behavioral abnormalities observed in CKO^{AST} mice, we used AAV-GfaABC1D-Cre to locally knock out astrocytic *Drd1* in the mPFC of *Drd1*$^{flox/flox}$ mice, and we conducted a series of behavioral tests (Fig. 6K−M). In the OFT, Cre mice spent more time in the center area without changes in total distance traveled (Fig. 6N−P). In the EPM test, Cre mice spent more time in the open arms (Fig. 6Q and R). In the FST, Cre mice exhibited a significant reduction in immobile time (Fig. 6S). In the Y-maze test, Cre mice presented a marked decrease in spontaneous alternation performance (Fig. 6T). These results indicate that astrocytic DRD1 in the mPFC are necessary for the regulation of anxiety-like behavior, passive coping responses, and cognitive function.

To investigate whether the increased D-serine levels in the mPFC may contribute to those behavioral changes in CKO^{AST} mice, control and CKO^{AST} mice received local injections of DAAO (0.1 unit/μL[76]) in the mPFC daily for two days before the experiment (Fig. 7A and B). The results showed that DAAO-treatment rescued anxiolytic-like behaviors and reduced passive coping response (Fig. 7C−G, Supporting Information Fig. S19). Additionally, treatment with DAAO eliminated the differences in Y-maze performance between CKO mice and control mice (Fig. 7H). These data suggest that D-serine contributes to behavioral modulation by the astrocytic DRD1.

In summary, our findings demonstrate that DRD1 on astrocytes in the PFC regulates excitatory synaptic transmission and synaptic plasticity by modulating extracellular levels of D-serine, which in turn affects emotional and cognitive functions (Fig. 7I).

4. Discussion

Dopamine is a key neuromodulator that regulates synaptic transmission and plasticity in the mPFC. In this study, we found that knockout of *Drd1* on astrocytes increased glutamatergic transmission and synaptic plasticity at the cellular level in the mPFC, and led to anxiolytic behavior, reduced passive coping responses, and impaired cognitive function at the behavioral level. *In vivo* microdialysis revealed elevated D-serine levels in the mPFC of astrocytic DRD1 knockout mice. Importantly, these cellular and behavioral changes were reversed by D-serine degrease treatment. Our findings demonstrate that astrocytic DRD1 in the PFC is crucial for regulating synaptic transmission and plasticity, as well as higher brain functions through D-serine.

Although DRD1 is also expressed on pyramidal neurons, we did not observe significant changes in spontaneous excitatory synaptic transmission in CKO^{PYR} mice. This finding may be explained by two factors. First, because electrophysiological recordings of coronal brain slices were performed, some neuronal terminals might have been severed during preparation. If DRD1-expressing pyramidal neurons are located presynaptically, this technical limitation may mask changes. Second, less than half of the pyramidal neurons in the mPFC express *Drd1*[37,77]. If DRD1-expressing pyramidal neurons are located postsynaptically, the limited proportion of these neurons may reduce the detectability of functional changes. Thus, we cannot rule out a regulatory role for DRD1 on pyramidal neurons in synaptic transmission.

The role of astrocytic DRD1 in regulating Ca^{2+} signaling has been debated. In juvenile mice, dopamine influences astrocytic Ca^{2+} signaling mainly through nondopaminergic receptors[44]. However, in adult mice, dopamine D1 and D2 receptors mediate this regulation[78]. Notably, DRD1 antagonists block dopamine-induced Ca^{2+} level elevations in astrocytes[78], which is consistent with our pharmacological experiment results and observations in adult transgenic mice (Fig. 1). Therefore, astrocytic DRD1 contributes to the regulation of astrocytic Ca^{2+} signaling in adult mice.

D-Serine, a key gliotransmitter, regulates synaptic transmission and plasticity[60,62,79], as well as systemic functions such as cognition[80], wakefulness[81], and the breathing response[82]. However, the upstream mechanisms controlling D-serine release remain unclear. Our study shows that astrocytic DRD1 regulates D-serine levels, likely by modulating serine racemase activity and vesicular release mechanisms.

PreNMDARs facilitate glutamate release at excitatory synapses[63,83], with D-serine serving as an essential coagonist[84]. We found that astrocytic DRD1 regulates extracellular D-serine,

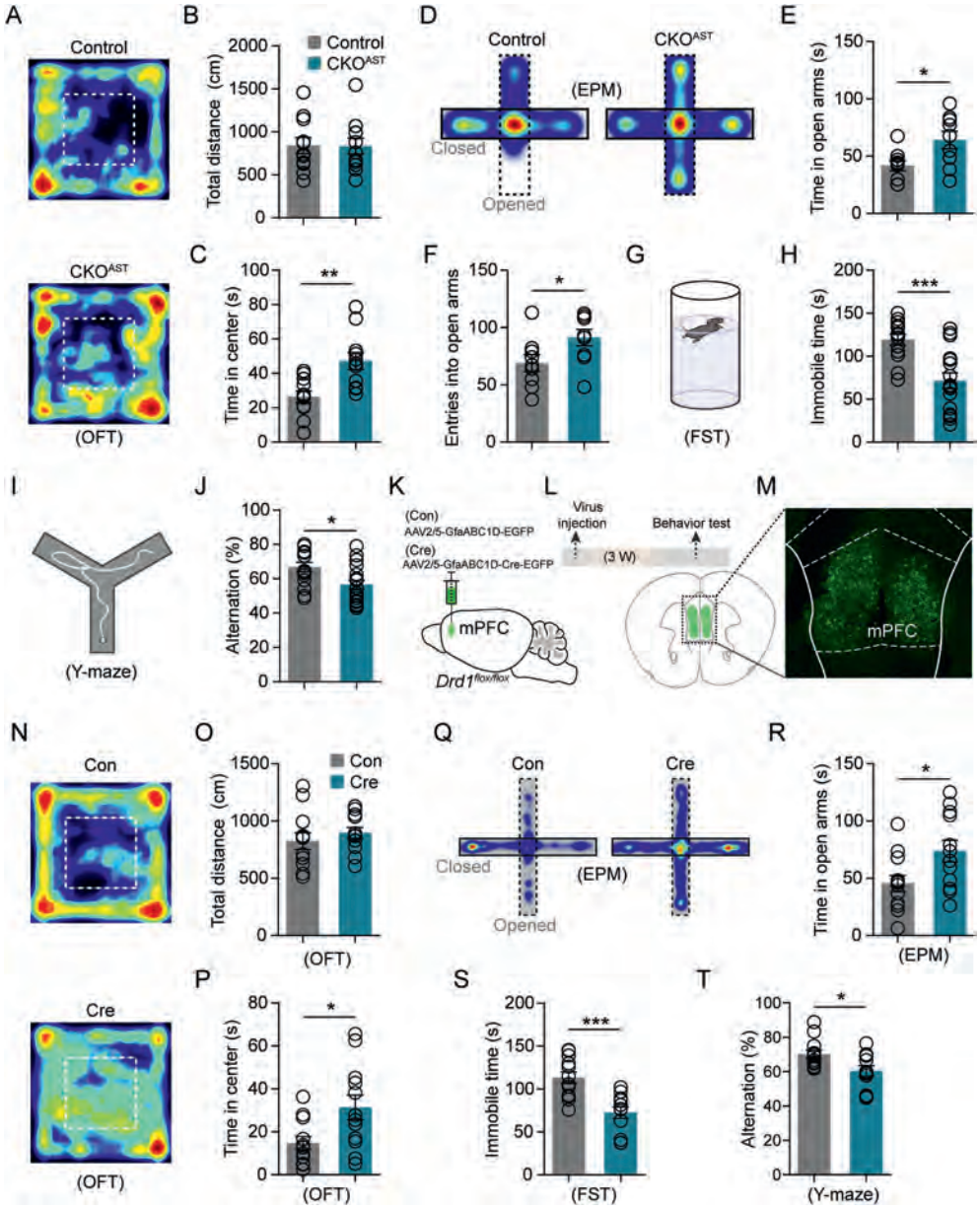

Figure 6 Astrocytic DRD1 in the mPFC modulates emotional and cognitive behaviors. (A−C) CKO^{AST} mice exhibited an anxiolytic phenotype compared to control mice in the open field test (OFT). (A) The representative heatmaps of two groups of mice in the OFT. Total distance (B) and time in center (C) from control and CKO^{AST} mice in the OFT. $n = 11$ mice from each group. C, Unpaired t test, $t = 3.47$, d$f = 20$, $P = 0.0024$. (D−F) CKO^{AST} mice exhibited an anxiolytic phenotype in the elevated plus maze (EPM) test. (D) The representative heatmaps of two groups of mice in the EPM test. Time in open arms (E) and entries in open arms (F) from control and CKO^{AST} mice in the EPM test. $n = 9$ mice from each group, E, Unpaired t test, $t = 2.545$, d$f = 16$, $P = 0.0216$, F, Unpaired t test, $t = 2.164$, d$f = 16$, $P = 0.0459$. (G) Schematic of the forced swimming test (FST). (H) CKO^{AST} mice exhibited a reduced passive coping response in the FST. $n = 14$ control mice and $n = 16$ CKO^{AST} mice, Unpaired t test, $t = 4.177$, d$f = 28$, $P = 0.0003$. (I) Schematic of the Y-maze test. (J) CKO^{AST} mice demonstrated a diminished capacity for alternation in the Y-maze test. $n = 17$ control mice and $n = 18$ CKO^{AST} mice, Unpaired t test, $t = 2.706$, d$f = 33$, $P = 0.0107$. (K−L) Schematic diagram of virus injection into the mPFC and experimental workflow. Con virus: AAV2/5-GfaABC1D-EGFP; Cre virus: AAV2/5-GfaABC1D-Cre-EGFP. (M) A representative image showing viral infection in the mPFC. (N) The representative heatmaps of two groups of mice in the OFT. (O, P) Cre mice exhibited anxiolytic-like behavior compared to con mice in the OFT. Total distance (O) and time in center (P) from Con and Cre mice in the OFT. $n = 12$ mice from each group. P, Unpaired t test with Welch's correction, $t = 2.556$, d$f = 16.67$, $P = 0.0207$. (Q) The representative heatmaps of two groups of mice in the EPM test. (R) Comparison of open arms time in the EPM test from Con and Cre mice. Unpaired t test, $t = 2.375$, d$f = 22$, $P = 0.0267$. (S) Immobile time in the FST from Con and Cre mice. Unpaired t test, $t = 4.266$, d$f = 22$, $P = 0.0003$. (T) Alternation in the Y-maze test from Con and Cre mice. Unpaired t test, $t = 2.473$, d$f = 22$, $P = 0.0216$. Statistical details are in the supplementary table. Data represent mean ± SEM, $*P < 0.05$, $**P < 0.01$, $***P < 0.001$. CKO^{AST}, astrocyte-specific *Drd1* knockout mice.

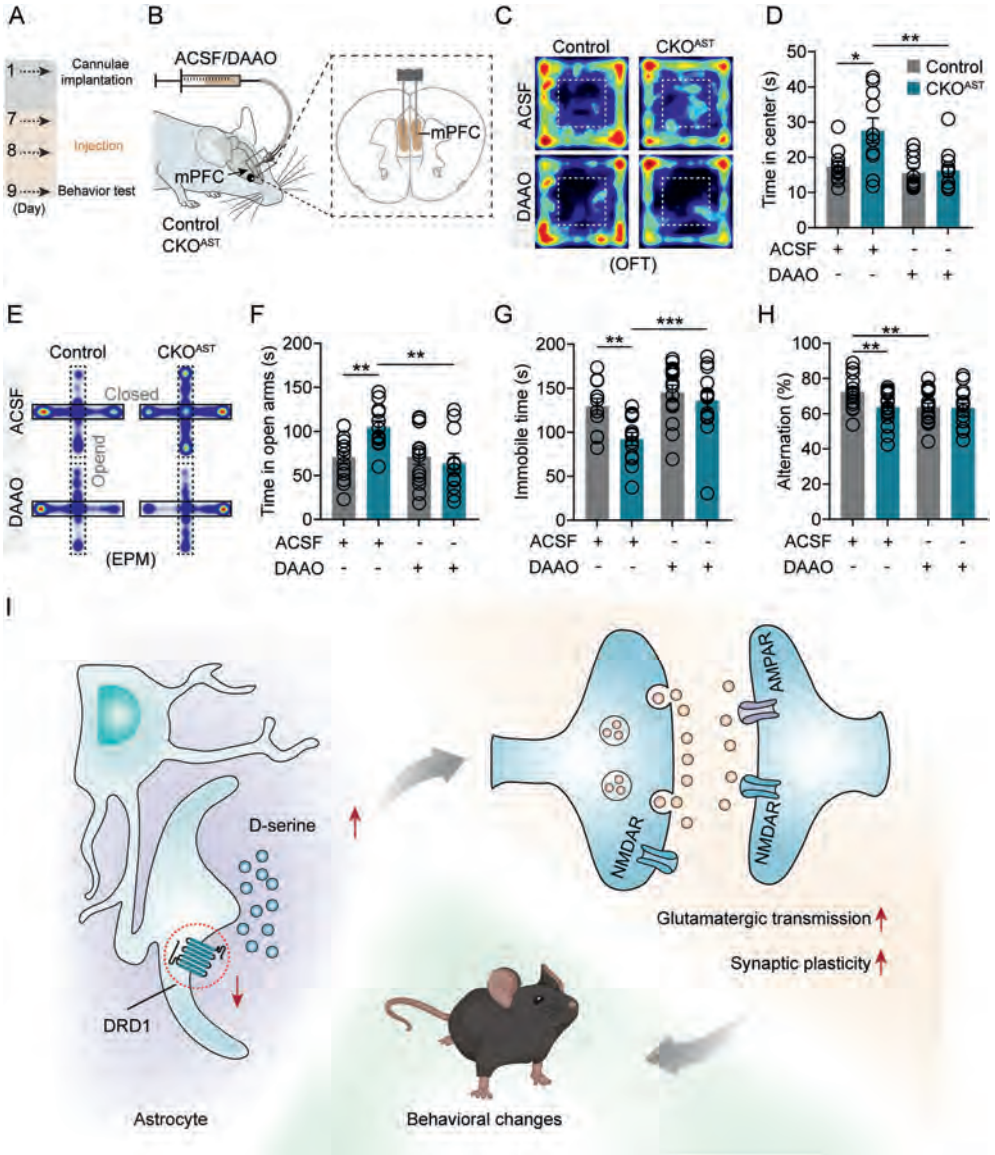

Figure 7 Astrocytic DRD1 in the mPFC modulates emotional and cognitive behaviors through D-serine. (A, B) Experimental workflow and schematic diagram of DAAO (D-amino acid oxidase, 0.1 unit/uL, 0.5 μL/side) injection into the mPFC. (C) The representative heatmaps of two groups of mice in the open field test (OFT). (D) Time in center from control and CKO^{AST} mice in the OFT after ACSF or DAAO injection into the mPFC. Control + ACSF: $n = 12$ mice, CKO^{AST} + ACSF: $n = 10$ mice, Control + DAAO: $n = 11$ mice, CKO^{AST} + DAAO: $n = 11$ mice. Control + ACSF *vs* CKO^{AST} + ACSF: Mann-Whitney test, $U = 27.5$, $P = 0.0309$; CKO^{AST} + ACSF *vs* CKO^{AST} + DAAO: Mann-Whitney test, $U = 18$, $P = 0.0079$. (E) The representative heatmaps of two groups of mice in the elevated plus maze (EPM) test . (F) Comparison of open arms time in the elevated plus maze after ACSF or DAAO injection into the mPFC in control and CKO^{AST} mice. Control + ACSF: $n = 14$ mice, CKO^{AST} + ACSF: $n = 12$ mice, Control + DAAO: $n = 14$ mice, CKO^{AST} + DAAO: $n = 11$ mice. Control + ACSF *vs* CKO^{AST} + ACSF: Unpaired *t* test, $t = 3.5$, d$f = 24$, $P = 0.0018$; CKO^{AST} + ACSF *vs* CKO^{AST} + DAAO: Unpaired *t* test, $t = 3.207$, d$f = 21$, $P = 0.0042$. (G) Immobile time in the forced swimming test (FST) after ACSF or DAAO injection into the mPFC from control and CKO^{AST} mice. Control + ACSF: $n = 11$ mice, CKO^{AST} + ACSF: $n = 13$ mice, Control + DAAO: $n = 16$ mice, CKO^{AST} + DAAO: $n = 15$ mice. Control + ACSF *vs* CKO^{AST} + ACSF: Unpaired *t* test, $t = 3.217$, d$f = 22$, $P = 0.004$; CKO^{AST} + ACSF *vs* CKO^{AST} + DAAO: Mann Whitney test, $U = 26$, $P = 0.0006$. (H) Alternation in the Y-maze test after ACSF or DAAO injection into the mPFC from control and CKO^{AST} mice. Control + ACSF: $n = 19$ mice, CKO^{AST} + ACSF: $n = 21$ mice, Control + DAAO: $n = 19$ mice, CKO^{AST} + DAAO: $n = 15$ mice. Control + ACSF *vs* CKO^{AST} + ACSF: Unpaired *t* test, $t = 2.982$, d$f = 38$, $P = 0.005$; Control + ACSF *vs* Control + DAAO: Unpaired *t* test, $t = 2.847$, d$f = 36$, $P = 0.0072$. (I) We hypothesize that the downregulation of DRD1 on astrocytes in the prefrontal cortex leads to an increase in extracellular levels of D-serine, which in turn enhances excitatory synaptic transmission and synaptic plasticity, ultimately resulting in behavioral changes such as anxiolytic-like behavior, reduced passive coping response, and impaired cognitive function. Statistical details are in the supplementary table. Data represent mean ± SEM, $^{*}P < 0.05$, $^{**}P < 0.01$, $^{***}P < 0.001$. DRD1, dopamine D1 receptor, CKO^{AST}, astrocyte-specific *Drd1* knockout mice.

thereby modulating excitatory transmission through preNMDARs. Although recordings were conducted at physiological Mg^{2+} levels, which typically block NMDARs at resting membrane potential, preNMDARs might be Mg^{2}-insensitive due to their unique subunit composition (*e.g.*, NR2C, NR2D, or NR3 subunits)[85,86]. Prior studies have functionally validated the presence of presynaptic NMDARs in cortical neurons[87], and the cortex expresses NR2C, NR2D, and NR3 receptor subunits[88-90], suggesting that presynaptic NMDARs may be insensitive to Mg^{2+} blockade[91]. Under the high-frequency stimulation used to induce LTP, Mg^{2+} can be expelled from postsynaptic NMDARs by depolarization, allowing D-serine to act on these activated receptors and contribute to the regulation of synaptic plasticity.

At the cellular level, reducing D-serine diminished excitatory synaptic transmission in control mice (Fig. 3I and J), but did not significantly alter emotional behavior (Fig. 7C−G). In contrast, CKO^{AST} mice exhibited both increased synaptic transmission and emotional abnormalities mediated by elevated D-serine levels. These findings suggest that emotional behavior may be more sensitive to elevated D-serine levels than to reduced D-serine levels in the mPFC. Interestingly, while increased LTP is typically associated with improved memory, knockout of astrocytic *Drd1* increased LTP but impaired cognitive performance. Consistently, prior studies have reported that excessive LTP in the mPFC[92], amygdala[93], and hippocampus[94,95] is associated with cognitive impairment. How changes at the cellular level affect outcomes at the behavioral level is currently unclear, but several possibilities may account for this phenomenon. First, the bidirectional regulation of synaptic strength-comprising both potentiation and suppression within a limited range-serves to maintain homeostasis, enhance storage capacity, reduce errors, and constrain the number and strength of potentiated synapses within an optimal window for memory storage[96-98]. Accordingly, moderate and physiologically enhanced synaptic plasticity is commonly associated with improved performance in cognitive tasks. However, when synaptic plasticity is excessively potentiated beyond the capacity of homeostatic regulation, this may impair the encoding and retrieval of information, manifesting behaviorally as learning deficits[93,95]. Second, while LTP is known to be NMDAR-dependent, some researchers propose that sustained activation of NMDAR-distinct from the transient activation observed during learning-may increase synaptic "noise" and thereby disrupt cognitive function[99]. Therefore, it is possible that aberrantly enhanced LTP and increased NMDAR activity in the CKO^{AST} mice may impair the acquisition and storage of new information. Notably, reducing D-serine levels abolished LTP induction (Fig. 3K) and impaired cognition (Fig. 7H), suggesting that both excessively high and low D-serine levels can cause cognitive dysfunction.

Given the widespread distribution and multiple roles of dopamine receptors, dysfunctions of the dopamine system have been implicated in various psychiatric disorders, including depression, schizophrenia, autism, attention deficit disorders, anxiety disorders[100-102], and cognitive disorders[103]. DRD1 is the most abundant dopamine receptor subtype, and their availability is reduced in patients with anxiety and major depressive disorders[101]. Although previous studies have shown that DRD1 in the PFC regulates emotional and cognitive functions[104-106], few studies have examined specific cell types, investigated the role of glial cells, or elucidated the underlying molecular mechanisms involved. Our study is the first to demonstrate that DRD1 on cortical glial cells regulates higher-order brain functions *via* D-serine, and therefore, these findings may provide new potential targets for the treatment of mental disorders.

5. Conclusions

We found that DRD1 on astrocytes in the PFC regulates excitatory synaptic transmission, synaptic plasticity, and emotional and cognitive functions by modulating D-serine levels. Our findings not only increase our understanding of the function of catecholamine receptors on astrocytes but also offer new potential avenues for the treatment of emotional and cognitive disorders.

Acknowledgements

We appreciate the technological support provided by Qianglong You, Jijong Liu, Song Lin and Weiyuan Huang from Southern Medical University (Guangzhou, China). This research was supported by grants from the National Key R&D Program of China (2022ZD0204700, 2021ZD0202700, 2022ZD0214300), National Natural Science Foundation of China (T2394535, 82090032, 32300968, and 32271014), Guangdong−Hong Kong Joint Laboratory for Psychiatric Disorders (2023B1212120004, China) and the Guangdong Basic and Applied Basic Research Foundation (2020A1515110565, China).

Author contributions

Tianming Gao, Yihua Chen and Yanan Yin designed the study. Yanan Yin and Jian Hu conducted the experiments with support from Haipeng Wu, Xinyu Yang, Jingwen Qi, Lang Huang, Zhengyi Luo, Shiyang Jin, Nengyuan Hu, Zhoucai Luo, Tong Luo, Hao Chen. Yanan Yin handled electrophysiological recordings and analysis, while Jian Hu performed and analyzed Ca^{2+} imaging and HPLC. Yanan Yin also analyzed the remaining data and prepared the figures. Technical support was provided by Xiaowen Li, Chunhua Yuan, Shuji Li, and Jianming Yang. Tianming Gao led the project and prepared the manuscript with the assistance of Yanan Yin, Yihua Chen and Jianming Yang.

Conflicts of interest

The authors declare that they have no conflicts of interest.

Appendix A. Supporting information

Supporting information to this article can be found online at https://doi.org/10.1016/j.apsb.2025.07.034.

References

1. Miller EK, Cohen JD. An integrative theory of prefrontal cortex function. *Annu Rev Neurosci* 2001;**24**:167−202.
2. Carlen M. What constitutes the prefrontal cortex?. *Science* 2017;**358**: 478−82.
3. Preuss TM, Wise SP. Evolution of prefrontal cortex. *Neuropsychopharmacology* 2021;**47**:3−19.
4. Donahue CJ, Glasser MF, Preuss TM, Rilling JK, Van Essen DC. Quantitative assessment of prefrontal cortex in humans relative to nonhuman primates. *Proc Natl Acad Sci U S A* 2018;**115**:E5183−92.
5. Ridderinkhof KR, Ullsperger M, Crone EA, Nieuwenhuis S. The role of the medial frontal cortex in cognitive control. *Science* 2004;**306**:443−7.

6. Spellman T, Rigotti M, Ahmari SE, Fusi S, Gogos JA, Gordon JA. Hippocampal-prefrontal input supports spatial encoding in working memory. *Nature* 2015;**522**:309−14.
7. Koechlin E, Summerfield C. An information theoretical approach to prefrontal executive function. *Trends Cognit Sci* 2007;**11**:229−35.
8. Eldridge MAG, Hines BE, Murray EA. The visual prefrontal cortex of anthropoids: interaction with temporal cortex in decision making and its role in the making of "visual animals". *Curr Opin Behav Sci* 2021;**41**:22−9.
9. Kim H, Ahrlund-Richter S, Wang X, Deisseroth K, Carlen M. Prefrontal parvalbumin neurons in control of attention. *Cell* 2016;**164**: 208−18.
10. Wu K, Wang D, Wang Y, Tang P, Li X, Pan Y, et al. Distinct circuits in anterior cingulate cortex encode safety assessment and mediate flexibility of fear reactions. *Neuron* 2023;**111**:3650−67.e6.
11. Mederos S, Sanchez-Puelles C, Esparza J, Valero M, Ponomarenko A, Perea G. GABAergic signaling to astrocytes in the prefrontal cortex sustains goal-directed behaviors. *Nat Neurosci* 2021;**24**:82−92.
12. Ito HT, Zhang SJ, Witter MP, Moser EI, Moser MB. A prefrontal-thalamo-hippocampal circuit for goal-directed spatial navigation. *Nature* 2015;**522**:50−5.
13. Hare BD, Duman RS. Prefrontal cortex circuits in depression and anxiety: contribution of discrete neuronal populations and target regions. *Mol Psychiatr* 2020;**25**:2742−58.
14. Dixon ML, Thiruchselvam R, Todd R, Christoff K. Emotion and the prefrontal cortex: an integrative review. *Psychol Bull* 2017;**143**: 1033−81.
15. Kouneiher F, Charron S, Koechlin E. Motivation and cognitive control in the human prefrontal cortex. *Nat Neurosci* 2009;**12**: 939−45.
16. Ferenczi EA, Zalocusky KA, Liston C, Grosenick L, Warden MR, Amatya D, et al. Prefrontal cortical regulation of brainwide circuit dynamics and reward-related behavior. *Science* 2016;**351**:aac9698.
17. Chocyk A, Majcher-Maslanka I, Dudys D, Przyborowska A, Wedzony K. Impact of early-life stress on the medial prefrontal cortex functions — a search for the pathomechanisms of anxiety and mood disorders. *Pharmacol Rep* 2013;**65**:1462−70.
18. Clauss JA, Benningfield MM, Rao U, Blackford JU. Altered prefrontal cortex function marks heightened anxiety risk in children. *J Am Acad Child Psychiatr* 2016;**55**:809−16.
19. Yan Z, Rein B. Mechanisms of synaptic transmission dysregulation in the prefrontal cortex: pathophysiological implications. *Mol Psychiatr* 2021;**27**:445−65.
20. Petrelli F, Dallerac G, Pucci L, Cali C, Zehnder T, Sultan S, et al. Dysfunction of homeostatic control of dopamine by astrocytes in the developing prefrontal cortex leads to cognitive impairments. *Mol Psychiatr* 2020;**25**:732−49.
21. Lei Y, Wang J, Wang D, Li C, Liu B, Fang X, et al. SIRT1 in forebrain excitatory neurons produces sexually dimorphic effects on depression-related behaviors and modulates neuronal excitability and synaptic transmission in the medial prefrontal cortex. *Mol Psychiatr* 2020;**25**:1094−111.
22. Klune CB, Jin B, DeNardo LA. Linking mPFC circuit maturation to the developmental regulation of emotional memory and cognitive flexibility. *eLife* 2021;**10**:e64567.
23. Brozoski TJ, Brown RM, Rosvold HE, Goldman PS. Cognitive deficit caused by regional depletion of dopamine in prefrontal cortex of rhesus monkey. *Science* 1979;**205**:929−32.
24. Tritsch NX, Sabatini BL. Dopaminergic modulation of synaptic transmission in cortex and striatum. *Neuron* 2012;**76**:33−50.
25. Leroi I, Barraclough M, McKie S, Hinvest N, Evans J, Elliott R, et al. Dopaminergic influences on executive function and impulsive behaviour in impulse control disorders in Parkinson's disease. *J Neuropsychol* 2013;**7**:306−25.
26. Schmack K, Bosc M, Ott T, Sturgill JF, Kepecs A. Striatal dopamine mediates hallucination-like perception in mice. *Science* 2021;**372**: eabf4740.
27. Sawaguchi T, Goldman-Rakic PS. D1 dopamine receptors in prefrontal cortex: involvement in working memory. *Science* 1991;**251**: 947−50.
28. Matthews GA, Nieh EH, Vander Weele CM, Halbert SA, Pradhan RV, Yosafat AS, et al. Dorsal raphe dopamine neurons represent the experience of social isolation. *Cell* 2016;**164**:617−31.
29. Zhang Y, Gao J, Li N, Xu P, Qu S, Cheng J, et al. Targeting cAMP in D1-MSNs in the nucleus accumbens, a new rapid antidepressant strategy. *Acta Pharm Sin B* 2024;**14**:667−81.
30. Seamans JK, Yang CR. The principal features and mechanisms of dopamine modulation in the prefrontal cortex. *Prog Neurobiol* 2004; **74**:1−58.
31. Vincent SL, Khan Y, Benes FM. Cellular distribution of dopamine D1 and D2 receptors in rat medial prefrontal cortex. *J Neurosci* 1993; **13**:2551−64.
32. Lidow MS, Wang F, Cao Y, Goldman-Rakic PS. Layer V neurons bear the majority of mRNAs encoding the five distinct dopamine receptor subtypes in the primate prefrontal cortex. *Synapse* 1998;**28**: 10−20.
33. Seamans JK, Durstewitz D, Christie BR, Stevens CF, Sejnowski TJ. Dopamine D1/D5 receptor modulation of excitatory synaptic inputs to layer V prefrontal cortex neurons. *Proc Natl Acad Sci U S A* 2001; **98**:301−6.
34. Gao WJ, Krimer LS, Goldman-Rakic PS. Presynaptic regulation of recurrent excitation by D1 receptors in prefrontal circuits. *Proc Natl Acad Sci U S A* 2001;**98**:295−300.
35. Harris KD, Shepherd GM. The neocortical circuit: themes and variations. *Nat Neurosci* 2015;**18**:170−81.
36. McKlveen JM, Moloney RD, Scheimann JR, Myers B, Herman JP. "Braking" the prefrontal cortex: the role of glucocorticoids and interneurons in stress adaptation and pathology. *Biol Psychiatry* 2019; **86**:669−81.
37. Santana N, Mengod G, Artigas F. Quantitative analysis of the expression of dopamine D1 and D2 receptors in pyramidal and GABAergic neurons of the rat prefrontal cortex. *Cerebr Cortex* 2009; **19**:849−60.
38. Smith SJ. Neural signalling. Neuromodulatory astrocytes. *Curr Biol* 1994;**4**:807−10.
39. Araque A, Parpura V, Sanzgiri RP, Haydon PG. Tripartite synapses: glia, the unacknowledged partner. *Trends Neurosci* 1999;**22**:208−15.
40. Perea G, Navarrete M, Araque A. Tripartite synapses: astrocytes process and control synaptic information. *Trends Neurosci* 2009;**32**: 421−31.
41. Shan LL, Zhang TR, Fan K, Cai WB, Liu HS. Astrocyte-neuron signaling in synaptogenesis. *Front Cell Dev Biol* 2021;**9**:680301.
42. Kofuji P, Araque A. G-Protein-Coupled receptors in astrocyte-neuron communication. *Neuroscience* 2021;**456**:71−84.
43. Ma W, Si T, Wang Z, Wen P, Zhu Z, Liu Q, et al. Astrocytic alpha4-containing nAChR signaling in the hippocampus governs the formation of temporal association memory. *Cell Rep* 2023;**42**:112674.
44. Pittolo S, Yokoyama S, Willoughby DD, Taylor CR, Reitman ME, Tse V, et al. Dopamine activates astrocytes in prefrontal cortex *via* alpha1-adrenergic receptors. *Cell Rep* 2022;**40**:111426.
45. Hu NY, Chen YT, Wang Q, Jie W, Liu YS, You QL, et al. Expression patterns of inducible cre recombinase driven by differential astrocyte-specific promoters in transgenic mouse lines. *Neurosci Bull* 2020;**36**:530−44.
46. Luo ZY, Huang L, Lin S, Yin YN, Jie W, Hu NY, et al. Erbin in amygdala parvalbumin-positive neurons modulates anxiety-like behaviors. *Biol Psychiatry* 2020;**87**:926−36.
47. Radzishevsky I, Wolosker H. An enzymatic-HPLC assay to monitor endogenous D-serine release from neuronal cultures. *Methods Mol Biol* 2012;**794**:291−7.
48. Lin LH, Wu QY, Zeng K, Chen ZY, Wang ZP, Li WM, et al. Medial amygdala NRG1 signaling mediates adolescent social isolation-induced autistic-like behaviors. *Sci Bull (Beijing)* 2024;**69**:1375−9.
49. Madisen L, Zwingman TA, Sunkin SM, Oh SW, Zariwala HA, Gu H, et al. A robust and high-throughput Cre reporting and

characterization system for the whole mouse brain. *Nat Neurosci* 2010;**13**:133−40.
50. Hu Z, Ma J, Gu Y. Lin28a is essential for synaptic plasticity in dentate granule cells and spatial memory. *Neurosci Bull* 2021;**37**: 261−6.
51. Li X, Du ZJ, Xu JN, Liang ZM, Lin S, Chen H, et al. mGluR5 in hippocampal CA1 pyramidal neurons mediates stress-induced anxiety-like behavior. *Neuropsychopharmacology* 2023;**48**:1164−74.
52. Cahill MK, Collard M, Tse V, Reitman ME, Etchenique R, Kirst C, et al. Network-level encoding of local neurotransmitters in cortical astrocytes. *Nature* 2024;**629**:146−53.
53. Handler A, Graham TGW, Cohn R, Morantte I, Siliciano AF, Zeng J, et al. Distinct dopamine receptor pathways underlie the temporal sensitivity of associative learning. *Cell* 2019;**178**:60−75.e19.
54. Bissiere S, Humeau Y, Luthi A. Dopamine gates LTP induction in lateral amygdala by suppressing feedforward inhibition. *Nat Neurosci* 2003;**6**:587−92.
55. Xu TX, Yao WD. D1 and D2 dopamine receptors in separate circuits cooperate to drive associative long-term potentiation in the prefrontal cortex. *Proc Natl Acad Sci U S A* 2010;**107**:16366−71.
56. Anderson MA, Burda JE, Ren Y, Ao Y, O'Shea TM, Kawaguchi R, et al. Astrocyte scar formation aids central nervous system axon regeneration. *Nature* 2016;**532**:195−200.
57. Li X, Zhong H, Wang Z, Xiao R, Antonson P, Liu T, et al. Loss of liver X receptor beta in astrocytes leads to anxiety-like behaviors *via* regulating synaptic transmission in the medial prefrontal cortex in mice. *Mol Psychiatr* 2021;**26**:6380−93.
58. Navarrete M, Araque A. Basal synaptic transmission: astrocytes rule. *Cell* 2011;**146**:675−7.
59. Araque A, Carmignoto G, Haydon PG, Oliet SH, Robitaille R, Volterra A. Gliotransmitters travel in time and space. *Neuron* 2014; **81**:728−39.
60. Panatier A, Theodosis DT, Mothet JP, Touquet B, Pollegioni L, Poulain DA, et al. Glia-derived D-serine controls NMDA receptor activity and synaptic memory. *Cell* 2006;**125**:775−84.
61. Mothet JP, Parent AT, Wolosker H, Brady Jr RO, Linden DJ, Ferris CD, et al. D-Serine is an endogenous ligand for the glycine site of the *N*-methyl-D-aspartate receptor. *Proc Natl Acad Sci U S A* 2000; **97**:4926−31.
62. Lench AM, Massey PV, Pollegioni L, Woodhall GL, Jones RS. Astroglial D-serine is the endogenous co-agonist at the presynaptic NMDA receptor in rat entorhinal cortex. *Neuropharmacology* 2014;**83**:118−27.
63. Yang J, Woodhall GL, Jones RS. Tonic facilitation of glutamate release by presynaptic NR2B-containing NMDA receptors is increased in the entorhinal cortex of chronically epileptic rats. *J Neurosci* 2006;**26**:406−10.
64. Yang Y, Ge W, Chen Y, Zhang Z, Shen W, Wu C, et al. Contribution of astrocytes to hippocampal long-term potentiation through release of D-serine. *Proc Natl Acad Sci U S A* 2003;**100**:15194−9.
65. Wolosker H. The neurobiology of D-serine signaling. *Adv Pharmacol* 2018;**82**:325−48.
66. Wolosker H, Mori H. Serine racemase: an unconventional enzyme for an unconventional transmitter. *Amino Acids* 2012;**43**:1895−904.
67. Foltyn VN, Zehl M, Dikopoltsev E, Jensen ON, Wolosker H. Phosphorylation of mouse serine racemase regulates D-serine synthesis. *FEBS Lett* 2010;**584**:2937−41.
68. Stamler JS, Lamas S, Fang FC. Nitrosylation. the prototypic redox-based signaling mechanism. *Cell* 2001;**106**:675−83.
69. Mustafa AK, Kumar M, Selvakumar B, Ho GP, Ehmsen JT, Barrow RK, et al. Nitric oxide *S*-nitrosylates serine racemase, mediating feedback inhibition of D-serine formation. *Proc Natl Acad Sci U S A* 2007;**104**:2950−5.
70. Mustafa AK, Ahmad AS, Zeynalov E, Gazi SK, Sikka G, Ehmsen JT, et al. Serine racemase deletion protects against cerebral ischemia and excitotoxicity. *J Neurosci* 2010;**30**:1413−6.
71. Martineau M, Parpura V, Mothet JP. Cell-type specific mechanisms of D-serine uptake and release in the brain. *Front Synaptic Neurosci* 2014;**6**:12.
72. Rosenberg D, Kartvelishvily E, Shleper M, Klinker CM, Bowser MT, Wolosker H. Neuronal release of D-serine: a physiological pathway controlling extracellular D-serine concentration. *FASEB J* 2010;**24**: 2951−61.
73. Mayanagi T, Yasuda H, Sobue K. PSD-Zip70 deficiency causes prefrontal hypofunction associated with glutamatergic synapse maturation defects by dysregulation of Rap2 activity. *J Neurosci* 2015;**35**:14327−40.
74. Friedman NP, Robbins TW. The role of prefrontal cortex in cognitive control and executive function. *Neuropsychopharmacology* 2022;**47**: 72−89.
75. Finn ES, Huber L, Jangraw DC, Molfese PJ, Bandettini PA. Layer-dependent activity in human prefrontal cortex during working memory. *Nat Neurosci* 2019;**22**:1687−95.
76. Cao S, Xiao Z, Sun M, Li Y. D-Serine in the midbrain periaqueductal gray contributes to morphine tolerance in rats. *Mol Pain* 2016;**12**: 1744806916646786.
77. Zhang ZW, Burke MW, Calakos N, Beaulieu JM, Vaucher E. Confocal analysis of cholinergic and dopaminergic inputs onto pyramidal cells in the prefrontal cortex of rodents. *Front Neuroanat* 2010;**4**:21.
78. Kim S, Kwon J, Park MG, Lee CJ. Dopamine-induced astrocytic Ca^{2+} signaling in mPFC is mediated by MAO-B in young mice, but by dopamine receptors in adult mice. *Mol Brain* 2022;**15**:90.
79. Henneberger C, Papouin T, Oliet SH, Rusakov DA. Long-term potentiation depends on release of D-serine from astrocytes. *Nature* 2010;**463**:232−6.
80. Koh W, Park M, Chun YE, Lee J, Shim HS, Park MG, et al. Astrocytes render memory flexible by releasing D-serine and regulating NMDA receptor tone in the Hippocampus. *Biol Psychiatry* 2022;**91**: 740−52.
81. Papouin T, Dunphy JM, Tolman M, Dineley KT, Haydon PG. Septal cholinergic neuromodulation tunes the astrocyte-dependent gating of hippocampal NMDA receptors to wakefulness. *Neuron* 2017;**94**: 840−54.e7.
82. Beltran-Castillo S, Olivares MJ, Contreras RA, Zuniga G, Llona I, von Bernhardi R, et al. D-Serine released by astrocytes in brainstem regulates breathing response to CO2 levels. *Nat Commun* 2017;**8**: 838.
83. Berretta N, Jones RS. Tonic facilitation of glutamate release by presynaptic *N*-methyl-D-aspartate autoreceptors in the entorhinal cortex. *Neuroscience* 1996;**75**:339−44.
84. Coyle JT, Balu D, Wolosker H. D-serine, the shape-shifting NMDA receptor Co-agonist. *Neurochem Res* 2020;**45**:1344−53.
85. Schwartz EJ, Rothman JS, Dugue GP, Diana M, Rousseau C, Silver RA, et al. NMDA receptors with incomplete Mg^{2+} block enable low-frequency transmission through the cerebellar cortex. *J Neurosci* 2012;**32**:6878−93.
86. Paoletti P, Bellone C, Zhou Q. NMDA receptor subunit diversity: impact on receptor properties, synaptic plasticity and disease. *Nat Rev Neurosci* 2013;**14**:383−400.
87. Buchanan KA, Blackman AV, Moreau AW, Elgar D, Costa RP, Lalanne T, et al. Target-specific expression of presynaptic NMDA receptors in neocortical microcircuits. *Neuron* 2012;**75**:451−66.
88. Karavanova I, Vasudevan K, Cheng J, Buonanno A. Novel regional and developmental NMDA receptor expression patterns uncovered in NR2C subunit-beta-galactosidase knock-in mice. *Mol Cell Neurosci* 2007;**34**:468−80.
89. Chen QY, Li XH, Lu JS, Liu Y, Lee JA, Chen YX, et al. NMDA GluN2C/2D receptors contribute to synaptic regulation and plasticity in the anterior cingulate cortex of adult mice. *Mol Brain* 2021;**14**:60.
90. Pachernegg S, Strutz-Seebohm N, Hollmann M. GluN3 subunit-containing NMDA receptors: not just one-trick ponies. *Trends Neurosci* 2012;**35**:240−9.
91. Abrahamsson T, Chou CYC, Li SY, Mancino A, Costa RP, Brock JA, et al. Differential regulation of evoked and spontaneous release by presynaptic NMDA receptors. *Neuron* 2017;**96**:839.

92. Baudin A, Blot K, Verney C, Estevez L, Santamaria J, Gressens P, et al. Maternal deprivation induces deficits in temporal memory and cognitive flexibility and exaggerates synaptic plasticity in the rat medial prefrontal cortex. *Neurobiol Learn Mem* 2012;**98**:207−14.
93. Lu Y, Sun XD, Hou FQ, Bi LL, Yin DM, Liu F, et al. Maintenance of GABAergic activity by neuregulin 1-ErbB4 in amygdala for fear memory. *Neuron* 2014;**84**:835−46.
94. Rutten K, Misner DL, Works M, Blokland A, Novak TJ, Santarelli L, et al. Enhanced long-term potentiation and impaired learning in phosphodiesterase 4D-knockout (PDE4D) mice. *Eur J Neurosci* 2008;**28**:625−32.
95. Migaud M, Charlesworth P, Dempster M, Webster LC, Watabe AM, Makhinson M, et al. Enhanced long-term potentiation and impaired learning in mice with mutant postsynaptic density-95 protein. *Nature* 1998;**396**:433−9.
96. Hancock PJB, Smith LS, Phillips WA. A biologically supported error-correcting learning rule. *Neural Comput* 1991;**3**:201−12.
97. Willshaw D, Dayan P. Optimal plasticity from matrix memories: what goes up must come down. *Neural Comput* 1990;**2**:85−93.
98. Sejnowski TJ. Statistical constraints on synaptic plasticity. *J Theor Biol* 1977;**69**:385−9.
99. Frankiewicz T, Parsons CG. Memantine restores long term potentiation impaired by tonic *N*-methyl-D-aspartate (NMDA) receptor activation following reduction of Mg^{2+} in hippocampal slices. *Neuropharmacology* 1999;**38**:1253−9.
100. Ayano G. Dopamine: receptors, functions, synthesis, pathways, locations and mental disorders: review of literatures. *J Ment Disord Treat* 2016;**2**:2.
101. Nikolaus S, Mamlins E, Hautzel H, Muller HW. Acute anxiety disorder, major depressive disorder, bipolar disorder and schizophrenia are related to different patterns of nigrostriatal and mesolimbic dopamine dysfunction. *Rev Neurosci* 2019;**30**:381−426.
102. Grace AA. Dysregulation of the dopamine system in the pathophysiology of schizophrenia and depression. *Nat Rev Neurosci* 2016; **17**:524−32.
103. Arnsten AF, Wang M, Paspalas CD. Dopamine's actions in primate prefrontal cortex: challenges for treating cognitive disorders. *Pharmacol Rev* 2015;**67**:681−96.
104. Beyer DKE, Mattukat A, Freund N. Prefrontal dopamine D1 receptor manipulation influences anxiety behavior and induces neuroinflammation within the hippocampus. *Int J Bipolar Disord* 2021;**9**:9.
105. Yang Y, Lee SM, Imamura F, Gowda K, Amin S, Mailman RB. D1 dopamine receptors intrinsic activity and functional selectivity affect working memory in prefrontal cortex. *Mol Psychiatr* 2021;**26**: 645−55.
106. Sun M, Zhang Y, Zhang XQ, Zhang Y, Wang XD, Li JT, et al. Dopamine D1 receptor in medial prefrontal cortex mediates the effects of TAAR1 activation on chronic stress-induced cognitive and social deficits. *Neuropsychopharmacology* 2024;**49**:1341−51.